

InfoBRIDGE: MUTUAL INFORMATION ESTIMATION VIA BRIDGE MATCHING

Sergei Kholkin

Applied AI Institute, Russia
kholkinsd@gmail.com

Ivan Butakov

Applied AI Institute, Russia,
MIRAI*, Russia
Institute of Numerical Mathematics (RAS),
Russia
ivan.butakov@applied-ai.ru

Evgeny Burnaev

Applied AI Institute, Russia,
AXXX, Russia
e.burnaev@applied-ai.ru

Nikita Gushchin

Applied AI Institute, Russia,
AXXX, Russia
i.nikita.gushchin@gmail.com

Alexander Korotin

Applied AI Institute, Russia,
AXXX, Russia
iamalexkorotin@gmail.com

ABSTRACT

Diffusion bridge models have recently become a powerful tool in the field of generative modeling. In this work, we leverage them to address another important problem in machine learning and information theory, the estimation of the mutual information (MI) between two random variables. Neatly framing MI estimation as a domain transfer problem, we construct an unbiased estimator for data posing difficulties for conventional MI estimators. We showcase the performance of our estimator on three standard MI estimation benchmarks, i.e., low-dimensional, image-based and high MI, and on real-world data, i.e., protein language model embeddings. The code for our estimator can be found at:

<https://github.com/SKholkin/infobridge>

1 INTRODUCTION

Information theory offers an extensive set of tools for quantifying probabilistic relations between random variables. It is widely used in machine learning for advanced statistical analysis (Berrett & Samworth, 2017; Sen et al., 2017; Duong & Nguyen, 2023b; Bounoua et al., 2024a), assessment of deep neural networks’ performance and generalization capabilities (Tishby & Zaslavsky, 2015; Xu & Raginsky, 2017; Goldfeld et al., 2019; Steinke & Zakyntinou, 2020; Amjad et al., 2022; Butakov et al., 2024b), self-supervised and semi-supervised learning (Linsker, 1988; Bell & Sejnowski, 1995; Hjelm et al., 2019; Stratos, 2019; Bachman et al., 2019; Veličković et al., 2019; van den Oord et al., 2019; Tschannen et al., 2020) and regularization or alignment in generative modeling (Chen et al., 2016; Belghazi et al., 2018; Ardizzone et al., 2020; Wang et al., 2024).

The majority of the aforementioned applications revolve around one of the central information-theoretic quantities – *mutual information* (MI). Due to several outstanding properties, MI is widely used as an invariant measure of non-linear dependence between random variables. Unfortunately, recent studies suggest that the curse of dimensionality is highly pronounced when estimating MI (Goldfeld et al., 2020; McAllester & Stratos, 2020). Additionally, it is argued that long tails, high values of MI and some other particular features of complex probability distributions can make mutual information estimation even more challenging (Czyż et al., 2023). On the other hand, recent developments in neural estimation methods demonstrate that sophisticated parametric estimators can achieve notable practical success in situations where traditional mutual information estimation techniques struggle (Belghazi et al., 2018; van den Oord et al., 2019; Song & Ermon, 2020; Rhodes et al., 2020; Ao & Li, 2022; Butakov et al., 2024a). Among neural estimators, generative approaches

*Moscow Independent Research Institute of Artificial Intelligence

are of particular interest, as they have proven to be effective in handling complex data (Duong & Nguyen, 2023a; Franzese et al., 2024; Butakov et al., 2024a). Since MI estimation is closely tied to approximation of a joint probability distribution, one can argue that leveraging state-of-the-art generative models, e.g., diffusion models, may result in additional performance gains.

Diffusion Bridge Matching. Diffusion models are a powerful type of generative models that show an impressive quality of image generation (Ho et al., 2020; Rombach et al., 2022). However, they have some disadvantages, such as the inability to perform data-to-data translation via diffusion. To tackle this problem, a novel promising approach based on Reciprocal Processes (Léonard et al., 2014) and Schrödinger Bridges (Schrödinger, 1932; Léonard, 2014a) has emerged. This approach is called the *diffusion bridge matching* and is used for learning generative diffusion processes for data-to-data translation. This type of model has shown itself as a powerful approach for numerous applications in biology (Tong et al., 2024; Bunne et al., 2023), chemistry (Somnath et al., 2023; Igashov et al., 2024), computer vision (Liu et al., 2023; Shi et al., 2023; Zhou et al., 2024), speech processing (Chen et al., 2023), unpaired learning (Shi et al., 2023; Gushchin et al., 2024b; 2023b;a; Ksenofontov & Korotin, 2025; Kholkin et al., 2026; Carrasco et al., 2026) and beyond (He et al., 2024; Gushchin et al., 2025).

Contributions. In this work, we employ the Diffusion Bridge Matching for the MI estimation.

1. **Theory.** We propose an unbiased mutual information estimator based on reciprocal processes, their diffusion representations and the Girsanov theorem (§4.1).
2. **Practice.** Building on the proposed theoretical framework and the powerful generative methodology of diffusion bridges, we develop a practical algorithm for MI estimation, named *InfoBridge* (§4.2). We demonstrate that our method achieves performance comparable to existing approaches on low-dimensional benchmarks and superior performance on image data benchmarks, protein embeddings data benchmark and high MI benchmark (§5).

Notations. We work in \mathbb{R}^D , which is the D -dimensional Euclidean space equipped with the Euclidean norm $\|\cdot\|$. We use $\mathcal{P}(\mathbb{R}^D)$ to denote the absolutely continuous Borel probability distributions whose variance and differential entropy are finite. To denote the density of $q \in \mathcal{P}(\mathbb{R}^D)$ at a point $x \in \mathbb{R}^D$, we use $q(x)$. We write $\text{KL}(\cdot\|\cdot)$ to denote the Kullback-Leibler divergence between two distributions. We denote the Dirac delta function as δ . We use Ω to denote the space of trajectories, i.e., continuous \mathbb{R}^D -valued functions of $t \in [0, 1]$. We write $\mathcal{P}(\Omega)$ to denote the probability distributions on the trajectories Ω whose marginals at $t = 0$ and $t = 1$ belong to $\mathcal{P}(\mathbb{R}^D)$; this is the set of stochastic processes. We use dW_t to denote the differential of the standard Wiener process $W \in \mathcal{P}(\Omega)$. We use $Q_{|x_0}$ and $Q_{|x_0, x_1}$ to denote the distribution of stochastic process Q conditioned on Q 's values x_0 and x_0, x_1 at times $t = 0$ and $t = 0, 1$, respectively. For a process $Q \in \mathcal{P}(\Omega)$, we denote its marginal distribution at time t by $q(x_t) \in \mathcal{P}(\mathbb{R}^D)$, and if the process is conditioned on its value x_s at time s , we denote the marginal distribution of such a process at time t by $q(x_t|x_s) \in \mathcal{P}(\mathbb{R}^D)$. SDE states for Stochastic Differential Equation (Øksendal, 2003, §5).

2 BACKGROUND

Mutual information. Information theory is a well-established framework for analyzing and quantifying interactions between random vectors. In this framework, mutual information (MI) serves as a fundamental and invariant measure of the non-linear dependence between two \mathbb{R}^D -valued random vectors X_0, X_1 . It is defined as follows:

$$I(X_0; X_1) \stackrel{\text{def}}{=} \text{KL}(\Pi_{X_0, X_1} \| \Pi_{X_0} \otimes \Pi_{X_1}), \quad (1)$$

where Π_{X_0, X_1} and Π_{X_0}, Π_{X_1} are the joint and marginal distributions of a pair of random vectors (X_0, X_1) . If the corresponding PDF $\pi(x_0, x_1)$ exists, the following also holds:

$$I(X_0; X_1) = \mathbb{E}_{\pi(x_0, x_1)} \log \frac{\pi(x_0, x_1)}{\pi(x_0)\pi(x_1)}. \quad (2)$$

Mutual information is symmetric, non-negative and equals zero if and only if X_0 and X_1 are independent. MI is also invariant to bijective mappings: $I(X_0; X_1) = I(g(X_0); X_1)$ if g^{-1} exists and g, g^{-1} are measurable (Cover & Thomas, 2006; Polyanskiy & Wu, 2024).

Brownian Bridge. Let W^ϵ be the Wiener process with a constant volatility $\epsilon > 0$, i.e., it is described by the SDE $dW^\epsilon = \sqrt{\epsilon}dW_t$, where W_t is the standard Wiener process. Let $W_{|x_0, x_1}^\epsilon$ denote the

process W^ϵ conditioned on its values x_0, x_1 at times $t = 0, 1$, respectively. This process $W_{|x_0, x_1}^\epsilon$ is called the Brownian Bridge (Ibe, 2013, Chapter 9).

Reciprocal processes. Reciprocal processes are a class of stochastic processes that have recently gained attention of research community in the contexts of stochastic optimal control (Léonard et al., 2014), Schrödinger Bridges (Schrödinger, 1932; Léonard, 2014a) and diffusion generative modeling (Liu et al., 2023; Gushchin et al., 2024a). In our paper, we consider a *particular case* of reciprocal processes which are induced by the Brownian Bridge $W_{|x_0, x_1}^\epsilon$.

Consider a joint distribution $\pi(x_0, x_1) \in \mathcal{P}(\mathbb{R}^{D \times 2})$ and define the process $Q_\pi \in \mathcal{P}(\Omega)$ as a mixture of Brownian bridges $W_{|x_0, x_1}^\epsilon$ with weights $\pi(x_0, x_1)$:

$$Q_\pi \stackrel{\text{def}}{=} \int W_{|x_0, x_1}^\epsilon d\pi(x_0, x_1).$$

This implies that to get trajectories of Q_π one has to first sample the start and end points, x_0 and x_1 , at times $t = 0$ and $t = 1$ from $\pi(x_0, x_1)$ and then simulate the Brownian Bridge $W_{|x_0, x_1}^\epsilon$. Notice that process Q_π depends on ϵ , but next in the paper we do not write ϵ and just stick to Q_π notation. Due to the non-causal nature of trajectory formation, such a process is, in general, non markovian. The set of all mixtures of Brownian Bridges can be described as:

$$\{Q \in \mathcal{P}(\Omega) \text{ s.t. } \exists \pi \in \mathcal{P}(\mathbb{R}^{D \times 2}) : Q = Q_\pi\}$$

and is called the set of *reciprocal processes* (for W^ϵ).

Reciprocal processes conditioned on the point. Consider a reciprocal process Q_π conditioned on some start point x_0 . Let the resulting process be denoted as $Q_{\pi|x_0}$, which remains reciprocal. Then process $Q_{\pi|x_0}$ is known as the Schrödinger Föllmer process (Vargas et al., 2023). While Q_π , in general, not markovian, $Q_{\pi|x_0}$ **is markovian**. Furthermore, if $\int_{\mathbb{R}^D} \|x_1\| d\pi(x_1) < \infty$, it is a diffusion process governed by the following SDE, i.e., see Proposition A.3:

$$\begin{aligned} Q_{\pi|x_0} : dx_t &= v_{x_0}(x_t, t)dt + \sqrt{\epsilon}dW_t, x_0 \sim \delta(x_0), \\ v_{x_0}(x_t, t) &= \mathbb{E}_{q_\pi(x_1|x_t, x_0)} \left[\frac{x_1 - x_t}{1 - t} \right]. \end{aligned} \quad (3)$$

Representations of reciprocal processes. The process Q_π can be naturally represented as a mixture of processes $Q_{\pi|x_0}$ conditioned on their starting points x_0 :

$$Q_\pi = \int Q_{\pi|x_0} d\pi(x_0).$$

Therefore, one may also express Q_π via an SDE but with non-markovian drift (conditioned on x_0):

$$\begin{aligned} Q_\pi : dx_t &= v(x_t, t, x_0)dt + \sqrt{\epsilon}dW_t, x_0 \sim \pi(x_0), \\ v(x_t, t, x_0) &= v_{x_0}(x_t, t) = \mathbb{E}_{q_\pi(x_1|x_t, x_0)} \left[\frac{x_1 - x_t}{1 - t} \right]. \end{aligned} \quad (4)$$

Conditional Bridge Matching. Although the drift $v_{x_0}(x_t, t)$ of $Q_{\pi|x_0}$ in (3) admits a closed form, it usually cannot be computed or estimated directly due to the unavailability of a way to easily sample from $\pi(x_1|x_t, x_0)$. However, it can be recovered by solving the following regression problem (Zhou et al., 2024):

$$v_{x_0} = \arg \min_u \mathbb{E}_{q_\pi(x_1, x_t|x_0), U_{[0,1]}(t)} \left\| \frac{x_1 - x_t}{1 - t} - u(x_t, t) \right\|^2, \quad (5)$$

where $U_{[0,1]}(t)$ denotes the uniform distribution over $t \in [0, 1]$, and the optimization is performed over drift functions $u : \mathbb{R}^D \times [0, 1] \rightarrow \mathbb{R}^D$. The same holds for the Q_π and its drift $v(x_t, t, x_0)$ through the addition of expectation w.r.t. $\pi(x_0)$:

$$v = \arg \min_u \mathbb{E}_{q_\pi(x_1, x_t|x_0)\pi(x_0), U_{[0,1]}(t)} \left\| \frac{x_1 - x_t}{1 - t} - u(x_t, t, x_0) \right\|^2 = \quad (6)$$

$$\arg \min_u \mathbb{E}_{q_\pi(x_1, x_t, x_0), U_{[0,1]}(t)} \left\| \frac{x_1 - x_t}{1 - t} - u(x_t, t, x_0) \right\|^2, \quad (7)$$

where $u : \mathbb{R}^D \times [0, 1) \times \mathbb{R}^D \rightarrow \mathbb{R}^D$. Problem (7) is usually solved with standard deep learning techniques. Namely, one parametrizes u with a neural network v_θ , and minimizes (7) using stochastic gradient descent and samples drawn from $q_\pi(x_0, x_t, x_1)$. The latter sampling is easy if one can sample from $\pi(x_0, x_1)$. Indeed, $q_\pi(x_0, x_t, x_1) = q_\pi(x_t | x_0, x_1) \pi(x_0, x_1)$, and one can sample first from $\pi(x_0, x_1)$ and then from $q_\pi(x_t | x_0, x_1)$, which is the time slice of the Brownian Bridge (Korotin et al., 2024, Eq 14), i.e., $W_{|x_0, x_1}^\epsilon(\cdot | t)$.

Such a procedure of learning drift v with a neural network is popular in generative modeling to solve a problem of sampling from conditional distribution $\pi(x_1 | x_0)$ and is frequently applied in the image-to-image transfer (Liu et al., 2023). The procedure of learning drift $v(x_t, t, x_0)$ (7) is usually called the *conditional* (or augmented) *bridge matching* (De Bortoli et al., 2023; Zhou et al., 2024). In addition, such procedure can also be derived through the well-celebrated Doob h -transform (De Bortoli et al., 2023; Palmowski & Rolski, 2002) or reversing a diffusion (Zhou et al., 2024).

3 RELATED WORK

Mutual information estimators. Mutual information estimators fall into two main categories: *non-parametric* and *parametric*. Parametric estimators are also subdivided into *discriminative* and *generative* (Song & Ermon, 2020; Federici et al., 2023). Beyond this natural categorization, we also distinguish *diffusion-based* approaches to better position our method w.r.t. prior work.

Non-parametric estimators. Classical MI estimation methods use non-parametric density estimators, such as kernel density estimation (Weglarczyk, 2018; Goldfeld et al., 2019) and k -nearest neighbors (Kozachenko & Leonenko, 1987; Kraskov et al., 2004; Berrett et al., 2019). The estimated densities are plugged into (2), and MI is computed via Monte Carlo integration. While appealing in low-dimensional settings, these approaches have been shown to fail on high-dimensional or complex data (Goldfeld et al., 2019, §5.3; Czyż et al., 2023, §6.2; Butakov et al., 2024a, Table 1).

Non-diffusion-based generative estimators. Parametric density models—such as normalizing flows and variational autoencoders—can be used to estimate MI via density estimation (Song & Ermon, 2020; McAllester & Stratos, 2020; Ao & Li, 2022; Duong & Nguyen, 2023a). However, results in (Song & Ermon, 2020, Figures 1,2) show that direct PDF estimation may introduce significant bias. To address this, recent works (Duong & Nguyen, 2023a; Butakov et al., 2024a; Dahlke & Pacheco, 2025) avoid PDF estimation and instead estimate the density ratio in (2), leveraging the invariance property of MI. While these methods perform better on synthetic benchmarks, they may still suffer from inductive biases introduced by simplified closed-form approximations.

Discriminative estimators. Another class of MI estimators relies on training a classifier to distinguish between samples from the joint distribution $\pi(x_0, x_1)$ and the product of marginals $\pi(x_0)\pi(x_1)$, as in MINE (Belghazi et al., 2018), InfoNCE (van den Oord et al., 2019), fDIME (Letizia et al., 2024) and SMILE (Song & Ermon, 2020). These approaches use variational bounds on KL divergence and offer parametric estimators suitable for high-dimensional and complex data. Despite their scalability, they suffer from well-known theoretical limitations, such as high variance in MINE and large batch size requirements in InfoNCE (Song & Ermon, 2020). Recent high-MI and complex distributions based benchmarks further indicate that discriminative methods may underperform compared to generative approaches (Franzese et al., 2024; Butakov et al., 2024a).

Neural Diffusion Estimator for MI (MINDE). One of the most recent generative methods for MI Estimation is diffusion-based (Song et al., 2021) MINDE (Franzese et al., 2024). To estimate $\text{KL}(\pi^A || \pi^B)$ the authors learn two standard backward diffusion models to generate data from distributions π^A and π^B , e.g., for π^A :

$$Q^A : \underbrace{dx_t = [-f(x_t, t) + g(t)^2 s^A(x_t, t)]dt + g(t)d\hat{W}_t}_{\text{backward diffusion}}, \quad x_T \sim q_T^A(x_T), \quad (8)$$

where f and g are the drift and volatility coefficients, respectively, of the forward diffusion (Song et al., 2021), $d\hat{W}_t$ is the Wiener process when time flows backwards, and q_t^A is the distribution of the noised data at time t (Franzese et al., 2024, §2, 3). The similar expressions hold for π^B and

Q^B . Then, the authors formulate a KL divergence estimator through the difference of diffusion *score functions*:

$$\text{KL}(\pi^A \parallel \pi^B) = \text{KL}(Q^A \parallel Q^B) = \int_0^T \mathbb{E}_{q_t^A(x_t)} \left[\frac{g(t)^2}{2} \|s^A(x_t, t) - s^B(x_t, t)\|^2 \right] dt + \text{KL}(q_T^A \parallel q_T^B) \quad (9)$$

Here, $\text{KL}(q_T^A \parallel q_T^B)$ is the **bias** term, which vanishes only when diffusion has infinitely many steps, i.e., $T \rightarrow \infty$. When the diffusion score functions s^A and s^B (8) are properly learned, one can draw samples from the forward diffusion $q_t^A(x_t) = q_t^A(x_t|x_0)q(x_0)$ and compute the estimate of KL divergence (9). In this way, the authors transform the problem of training the KL divergence estimator into the problem of learning the backward diffusions (8) that generate *data from noise*.

To estimate **mutual information**, the authors propose a total of four equivalent methods, all based on the estimation of up to three KL divergences (9) or their expectations.

4 InfoBRIDGE MUTUAL INFORMATION ESTIMATOR

In (§4.1), we propose our novel MI estimator which is based on difference of diffusion drifts of conditional reciprocal processes. We explain the practical learning procedure in (§4.2) and suggest some straightforward generalizations of our method in (§4.3).

4.1 COMPUTING MI THROUGH RECIPROCAL PROCESSES

Consider the problem of MI estimation for random variables X_0 and X_1 with joint distribution $\pi(x_0, x_1)$. To tackle this problem, we employ reciprocal processes:

$$Q_\pi \stackrel{\text{def}}{=} \int W_{|x_0, x_1}^\epsilon d\pi(x_0, x_1), Q_\pi^{\text{ind}} \stackrel{\text{def}}{=} \int W_{|x_0, x_1}^\epsilon d\pi(x_0) d\pi(x_1). \quad (10)$$

We show that the KL between the distributions $\pi(x_0, x_1)$ and $\pi(x_0)\pi(x_1)$ (1) is equal to the KL between the reciprocal processes Q_π and Q_π^{ind} , and decompose the latter into the difference of drifts.

First, let us introduce a classical stochastic calculus result that allows us to compute the KL between diffusion processes, e.g., Q_π and Q_π^{ind} SDE representations.

KL divergence between diffusion processes. Consider two diffusion processes with the same volatility coefficient $\sqrt{\epsilon}$ that start at the same distribution π_0 :

$$Q^\alpha : dx_t = f^\alpha(x_t, t) dt + \sqrt{\epsilon} dW_t, \quad x_0 \sim \pi_0(x_0), \quad \alpha \in \{A, B\}. \quad (11)$$

By the application of the disintegration theorem (Léonard, 2014b, §1) and the Girsanov theorem (Léonard, 2012) one can derive the KL divergence between these diffusions:

$$\text{KL}(Q^A \parallel Q^B) = \frac{1}{2\epsilon} \int_0^1 \mathbb{E}_{q^A(x_t)} [\|f^A(x_t, t) - f^B(x_t, t)\|^2] dt, \quad (12)$$

where $q^A(x_t)$ is the marginal distribution of Q^A at time t .

This allows one to estimate the KL divergence between two diffusions with the same volatility coefficient and the same initial distributions, knowing only their *drifts* and marginal samples $x_t \sim q^A(x_t)$. This fact is widely used in Bridge Matching (Shi et al., 2023; Peluchetti, 2023), Diffusion (Franzese et al., 2024) and Schrödinger Bridge Models (Vargas et al., 2021; Gushchin et al., 2023a).

Theorem 4.1 (Mutual Information decomposition). *Consider random variables X_0, X_1 and their joint distribution $\pi(x_0, x_1)$, such that $I(X_0; X_1) < \infty$ and $\int_{\mathbb{R}^D} \|x_1\| d\pi(x_1) < \infty$. Consider reciprocal processes $Q_\pi, Q_\pi^{\text{ind}}$ induced by distributions $\pi(x_0, x_1)$ and $\pi(x_0)\pi(x_1)$, respectively, as in (10). Then the MI between the random variables X_0 and X_1 can be expressed as:*

$$I(X_0; X_1) = \frac{1}{2\epsilon} \int_0^1 \mathbb{E}_{q_\pi(x_t, x_0)} \|v_{\text{joint}}(x_t, t, x_0) - v_{\text{ind}}(x_t, t, x_0)\|^2 dt, \quad (13)$$

where

$$v_{\text{joint}}(x_t, t, x_0) = \mathbb{E}_{q_\pi(x_1|x_t, x_0)} \left[\frac{x_1 - x_t}{1 - t} \right], \quad (14)$$

$$v_{\text{ind}}(x_t, t, x_0) = \mathbb{E}_{q_\pi^{\text{ind}}(x_1|x_t, x_0)} \left[\frac{x_1 - x_t}{1 - t} \right]. \quad (15)$$

v_{joint} and v_{ind} are the drifts of the SDE representations (4) of the reciprocal processes Q_π and Q_π^{ind} .

Algorithm 1: *InfoBridge*. Training the model.

Input : Distribution $\pi(x_0, x_1)$ accessible by samples, initial neural network parametrization v_θ of drift functions

Output : Learned neural network v_θ approximating drifts v_{joint} and v_{ind}

repeat

 Sample batch of pairs $\{x_0^n, x_1^n\}_{n=0}^N \sim \pi(x_0, x_1)$;
 Sample random permutation $\{\hat{x}_1^n\}_{n=0}^N = \text{Permute}(\{x_1^n\}_{n=0}^N)$;
 Sample batch $\{t^n\}_{n=1}^N \sim U[0, 1]$;
 Sample batch $\{x_t^n\}_{n=1}^N \sim W_{|x_0, x_1}^\epsilon$;
 Sample batch $\{\hat{x}_t^n\}_{n=1}^N \sim W_{|x_0, \hat{x}_1}^\epsilon$;
 $\mathcal{L}_\theta^1 = \frac{1}{N} \sum_{n=1}^N \|v_\theta(x_t^n, t^n, x_0^n, 1) - \frac{x_1^n - x_t^n}{1 - t^n}\|^2$;
 $\mathcal{L}_\theta^2 = \frac{1}{N} \sum_{n=1}^N \|v_\theta(\hat{x}_t^n, t^n, x_0^n, 0) - \frac{\hat{x}_1^n - \hat{x}_t^n}{1 - t^n}\|^2$;
 Update θ using $\frac{\partial \mathcal{L}_\theta^1}{\partial \theta} + \frac{\partial \mathcal{L}_\theta^2}{\partial \theta}$;

until converged;

Algorithm 2: *InfoBridge*. MI estimator.

Input : Distribution $\pi(x_0, x_1)$ accessible by samples, neural network parametrization v_θ of drift functions approximating optimal drifts v_{joint} and v_{ind} , number of samples N

Output : Mutual information estimation $\widehat{\text{MI}}$

 Sample batch of pairs $\{x_0^n, x_1^n\}_{n=1}^N \sim \pi(x_0, x_1)$;
 Sample batch $\{t^n\}_{n=1}^N \sim U_{[0,1]}(t)$;
 Sample batch $\{x_t^n\}_{n=1}^N \sim W_{|x_0, x_1}^\epsilon(\cdot | \{t^n\}_{n=1}^N)$;
 $\widehat{\text{MI}} \leftarrow \frac{1}{2\epsilon N} \sum_{n=0}^N \|v_\theta(x_t^n, t^n, x_0^n, 1) - v_\theta(x_t^n, t^n, x_0^n, 0)\|^2$

Proof sketch: Starting from the quantity $\text{KL}(Q_\pi \| Q_\pi^{\text{ind}})$, we first apply the disintegration theorem to express it as $\mathbb{E}_{\pi(x_0)}[\text{KL}(Q_{\pi|x_0} \| Q_{\pi|x_0}^{\text{ind}})]$ and apply it one more time to express it as $\text{KL}(\pi(x_0, x_1) \| \pi(x_0)\pi(x_1))$. Finally, we decompose the KL between the conditional diffusion processes $\text{KL}(Q_{\pi|x_0} \| Q_{\pi|x_0}^{\text{ind}})$ using Girsanov’s theorem. Full proof is provided in Section A.

Once the drifts v_{joint} and v_{ind} are known, our Theorem 4.1 provides a straightforward way to estimate the mutual information between the random variables X_0 and X_1 by evaluating the difference between the drifts $v_{\text{joint}}(x_t, t, x_0)$ (14) and $v_{\text{ind}}(x_t, t, x_0)$ (15) at points x_0, x_t sampled from the distribution of the reciprocal process Q_π at times 0, t . Regularity assumptions (Shi et al., 2023, Appendix C) are relatively mild and common for diffusion bridges generative modeling, i.e., they include restrictions such as finite first moment.

Remark. Our approach is different from MINDE, because we frame MI estimation as a **domain transfer** task, while MINDE frames it as **generative modeling** task. Our formulation allows **unbiased**¹ MI estimation (13) while MINDE has non zero bias term (9). Furthermore, the domain transfer perspective yields easier to learn trajectories and reduced variance in MI estimation Tables 2 and 3. More details on the comparison with MINDE are presented in the Appendix C.

4.2 *InfoBRIDGE*. PRACTICAL OPTIMIZATION PROCEDURE

The drifts v_{joint} and v_{ind} of reciprocal processes Q_π and Q_π^{ind} can be recovered by the conditional Bridge Matching procedure, see (7). We have to solve optimization problem (7) by parametrizing v_{joint} and v_{ind} with neural networks $v_{\text{joint}, \phi}$ and $v_{\text{ind}, \psi}$, respectively, and applying Stochastic Gradient Descent on Monte Carlo approximation of (7). The sampling from the distribution $q_\pi(x_t, x_0)$ of reciprocal process Q_π at times 0, t is easy because:

$$q_\pi(x_t, x_0) = \mathbb{E}_{q_\pi(x_1)}[q_\pi(x_t, x_0 | x_1)] = \mathbb{E}_{q_\pi(x_1)}[q_\pi(x_t | x_1, x_0)\pi(x_0 | x_1)].$$

¹In our case, by the word *unbiased* we mean that under full access to distributions and under the assumption that we can learn drift functions ideally, the estimation of the objective is unbiased.

Table 1: Mean MI estimates over 10 seeds using 10k test samples against ground truth (GT), adopted from Franzese et al. (2024). The closer the estimate is to the ground truth, the better. Color indicates relative negative (red) and positive bias (blue).

GT	Method Type	0.2	0.4	0.3	0.4	0.4	0.4	0.4	1.0	1.0	1.0	1.0	0.3	1.0	1.3	1.0	0.4	1.0	0.6	1.6	0.4	1.0	1.0	1.0	1.0	1.0	1.0	1.0	1.0	0.2	0.4	0.2	0.3	0.2	0.4	0.3	0.4	1.7	0.3	0.4	
InfoBridge(ours)	Bridge Matching	0.3	0.5	0.3	0.4	0.4	0.4	0.9	1.0	1.0	1.0	0.3	1.0	1.3	1.0	0.4	1.0	0.6	1.7	0.4	1.0	1.0	1.0	1.0	0.9	0.9	1.0	1.0	1.0	0.0	0.0	0.2	0.3	0.2	0.5	0.3	0.5	1.3	0.4	0.4	
NVF	Flow	0.2	0.4	0.3	0.6	0.4	0.4	0.4	1.0	1.0	1.0	1.0	0.3	1.0	1.3	1.0	0.4	1.0	0.6	1.5	0.4	1.0	1.0	1.0	0.8	0.5	0.6	0.9	1.0	1.0	∞	∞	∞	0.5	0.2	0.4	0.4	1.5	0.2	0.4	
JVF	Flow	0.0	0.0	0.0	0.0	0.0	0.4	0.4	1.0	1.0	1.0	1.0	0.3	1.0	1.3	1.0	0.4	1.0	0.6	1.6	0.4	1.0	1.0	1.0	0.8	0.3	0.4	1.0	0.9	0.9	1.8	2.7	0.0	1.0	0.1	0.0	0.0	1.6	0.2	0.4	
MINDE-j	Diffusion	0.2	0.4	0.3	0.4	0.4	0.4	1.2	1.0	1.0	1.0	0.3	1.0	1.3	1.0	0.4	1.0	0.6	1.7	0.4	1.1	1.0	1.0	1.0	0.9	0.9	1.1	1.0	1.0	0.1	0.2	0.2	0.3	0.2	0.5	0.3	0.4	1.7	0.3	0.4	
MINDE-c	Diffusion	0.2	0.4	0.3	0.4	0.4	0.4	1.0	1.0	1.0	1.0	0.3	1.0	1.3	1.0	0.4	1.0	0.6	1.6	0.4	1.0	1.0	1.0	0.9	0.9	0.9	1.0	1.0	1.0	0.1	0.3	0.2	0.3	0.2	0.4	0.3	0.4	1.7	0.3	0.4	
MINE		0.2	0.4	0.2	0.4	0.4	0.4	1.0	1.0	1.0	1.0	0.3	1.0	1.3	1.0	0.4	1.0	0.6	1.6	0.4	0.9	0.9	0.9	0.8	0.7	0.6	0.9	0.9	0.9	0.0	0.0	0.1	0.1	0.1	0.2	0.2	0.4	1.7	0.3	0.4	
InfoNCE		0.2	0.4	0.3	0.4	0.4	0.4	1.0	1.0	1.0	1.0	0.3	1.0	1.3	1.0	0.4	1.0	0.6	1.6	0.4	0.9	1.0	1.0	0.8	0.8	0.8	0.9	1.0	1.0	0.2	0.3	0.2	0.3	0.2	0.4	0.3	0.4	1.7	0.3	0.4	
DoE (Gaussian)		0.2	0.5	0.3	0.6	0.4	0.4	0.7	1.0	1.0	1.0	0.4	0.7	7.8	1.0	0.6	0.9	1.3	0.4	0.7	1.0	1.0	0.5	0.6	0.6	0.6	0.7	0.8	6.7	7.9	1.8	2.5	0.6	4.2	1.2	1.6	0.1	0.4			
DoE (Logistic)	Classical	0.1	0.4	0.2	0.4	0.4	0.4	0.6	0.9	0.9	1.0	0.3	0.7	7.8	1.0	0.6	0.9	1.3	0.4	0.8	1.1	1.0	0.5	0.6	0.6	0.7	0.8	0.8	0.5	0.8	0.3	1.5	0.6	1.6	0.1	0.4					
KSG		0.2	0.4	0.2	0.2	0.4	0.4	0.4	0.2	0.9	0.7	1.0	0.3	0.2	1.1	1.0	0.4	0.7	0.6	1.3	0.4	0.2	0.9	0.7	0.2	0.7	0.6	0.2	0.9	0.7	0.2	0.2	0.1	0.1	0.1	0.2	0.2	0.4	1.7	0.3	0.4

Wiggly @ Bivariate $M_n 1 \times 1$
Uniform 1×1 (additive noise=0.75)
Uniform 1×1 (additive noise=0.1)
Swiss roll 2×1
 $S^5 \times 5$ (ddof=3)
 $S^5 \times 5$ (ddof=2)
 $S^3 \times 3$ (ddof=3)
 $S^3 \times 3$ (ddof=2)
 $S^2 \times 2$ (ddof=2)
 $S^2 \times 2$ (ddof=1)
 $S^1 \times 1$ (ddof=1)
Sp @ Min CDF @ $M_n 5 \times 5$ (2-pair)
Sp @ Min CDF @ $M_n 3 \times 3$ (2-pair)
Sp @ Min CDF @ $M_n 25 \times 25$ (2-pair)
Sp @ Min 5×5 (2-pair)
Sp @ Min 3×3 (2-pair)
Sp @ Min 25×25 (2-pair)
Min CDF @ $M_n 5 \times 5$ (2-pair)
Min CDF @ $M_n 3 \times 3$ (2-pair)
Min CDF @ $M_n 25 \times 25$ (2-pair)
Bivariate $M_n 1 \times 1$
Min 50×50 (dense)
Min 5×5 (dense)
Min 5×5 (2-pair)
Min 3×3 (dense)
Min 3×3 (2-pair)
Min 25×25 (dense)
Min 25×25 (2-pair)
Min 2×2 (dense)
Min 2×2 (2-pair)
Hc @ Min 5×5 (2-pair)
Hc @ Min 3×3 (2-pair)
Hc @ Min 25×25 (2-pair)
Bivariate $M_n 1 \times 1$
Bimodal 1×1
Ashih @ $S^5 \times 5$ (ddof=2)
Ashih @ $S^3 \times 3$ (ddof=2)
Ashih @ $S^2 \times 2$ (ddof=1)
Ashih @ $S^1 \times 1$ (ddof=1)

Wiggly @ Bivariate $M_n 1 \times 1$
Uniform 1×1 (additive noise=0.75)
Uniform 1×1 (additive noise=0.1)
Swiss roll 2×1
 $S^5 \times 5$ (ddof=3)
 $S^5 \times 5$ (ddof=2)
 $S^3 \times 3$ (ddof=3)
 $S^3 \times 3$ (ddof=2)
 $S^2 \times 2$ (ddof=2)
 $S^2 \times 2$ (ddof=1)
 $S^1 \times 1$ (ddof=1)
Sp @ Min CDF @ $M_n 5 \times 5$ (2-pair)
Sp @ Min CDF @ $M_n 3 \times 3$ (2-pair)
Sp @ Min CDF @ $M_n 25 \times 25$ (2-pair)
Sp @ Min 5×5 (2-pair)
Sp @ Min 3×3 (2-pair)
Sp @ Min 25×25 (2-pair)
Min CDF @ $M_n 5 \times 5$ (2-pair)
Min CDF @ $M_n 3 \times 3$ (2-pair)
Min CDF @ $M_n 25 \times 25$ (2-pair)
Bivariate $M_n 1 \times 1$
Min 50×50 (dense)
Min 5×5 (dense)
Min 5×5 (2-pair)
Min 3×3 (dense)
Min 3×3 (2-pair)
Min 25×25 (dense)
Min 25×25 (2-pair)
Min 2×2 (dense)
Min 2×2 (2-pair)
Hc @ Min 5×5 (2-pair)
Hc @ Min 3×3 (2-pair)
Hc @ Min 25×25 (2-pair)
Bivariate $M_n 1 \times 1$
Bimodal 1×1
Ashih @ $S^5 \times 5$ (ddof=2)
Ashih @ $S^3 \times 3$ (ddof=2)
Ashih @ $S^2 \times 2$ (ddof=1)
Ashih @ $S^1 \times 1$ (ddof=1)

Therefore, to sample from $q_\pi(x_t, x_0)$ it suffices to sample $x_0, x_1 \sim \pi(x_0, x_1)$ and sample from $q_\pi(x_t|x_1, x_0)$ which is again just a Brownian Bridge.

Vector field parametrization. In practice, we replace two separate neural networks that approximate the drifts $v_{\text{joint}}(x_t, t, x_0)$ and $v_{\text{ind}}(x_t, t, x_0)$ with a single neural network that incorporates an additional binary input. Specifically, we introduce a binary input $s \in \{0, 1\}$ to unify the drift approximations in the following way: $v_\theta(\cdot, 1) \approx v_{\text{joint}}(\cdot)$ and $v_\theta(\cdot, 0) \approx v_{\text{ind}}(\cdot)$. Such binary conditioning is widely used for the conditioning of diffusion (Ho & Salimans, 2021) and bridge matching (Bortoli et al., 2024) models. In Appendix C.5 we show that it provides a more accurate estimation.

We call our practical MI estimation algorithm **InfoBridge**. The drifts v_θ training procedure is described in Algorithm 1 and the MI estimation procedure is described in Algorithm 2. One can see that both model training and MI estimation procedures are simulation-free.

Several strategies exist for sampling data used in computing the independent drift loss \mathcal{L}_θ^2 in Algorithm 1. While regular permutation works well in practice, it may introduce correlations (Letizia et al., 2024). Alternatives include “derangement” permutations (Letizia et al., 2024) or resampling from the marginal. See Appendix C.4 for further discussion.

The computational complexity of our algorithm as a Diffusion Bridge model is greater than that of discriminative methods and is similar to that of MINDE.

4.3 GENERALIZATIONS AND IMPLICATIONS

Generalizations. Our method admits several straightforward extensions. For completeness, we present a method for the unbiased estimation of the general KL divergence in Appendix B.1. According to Theorem B.1 the KL divergence between any two distributions can be decomposed into the difference of diffusion drifts in a similar way to (13).

Furthermore, our method can be extended to estimation of MI between random variables of different dimensionality (Appendix B.5) and naturally generalizes to the estimation of mutual information involving more than two random variables, known as **interaction information** (Appendix B.4). Practical procedures for these generalizations can also be derived in a similar way to (§4.2).

Generative byproduct. Note that the learned drifts $v_\theta(\cdot, 1)$ and $v_\theta(\cdot, 0)$ define the distributions $\pi_{\theta, \text{joint}}(x_1|x_0) \approx \pi(x_1|x_0)$ and $\pi_{\theta, \text{ind}}(x_1|x_0) \approx \pi(x_1)$ as solutions to the corresponding SDEs (4). One can simulate these SDEs by utilizing diffusion based generative modeling methods. Samples from $\pi_{\theta, \text{joint}}(x_1|x_0)$ and $\pi_{\theta, \text{ind}}(x_1|x_0)$ for the image based benchmark (Section 5.2) can be seen at Figure 5. This is unnecessary for the MI estimation, but can be considered as an additional feature.

5 EXPERIMENTS

We test our method on a diverse set of benchmarks with known ground truth values of mutual information. To cover low-dimensional cases and some basic cases of data lying on a manifold, we employ the tests by (Czyż et al., 2023). Benchmarks from (Butakov et al., 2024b;a) are used to assess the method on manifolds represented as images. To evaluate our method on real-world data, we use protein language model embeddings and adopt the benchmark construction procedure proposed in (Lee & Rhee, 2024). Finally, we evaluate our method on high mutual information tasks from (Czyż et al., 2023). In addition, we present an ablation study in Appendix C.2, analyzing the impact of key hyperparameters, including the volatility coefficient ϵ , neural network architectures. We compare our method with a diverse collection of other MI estimation methods: diffusion based MINDE (Franzese et al., 2024), flow-based NVF, JVF (Dahlke & Pacheco, 2025), MIENF (Butakov et al., 2024a), classical MINE (Belghazi et al., 2018), InfoNCE (van den Oord et al., 2019), fDIME (Letizia et al., 2024), NWJ (Nguyen et al., 2010), KSG (Kraskov et al., 2004).

Across all four experimental setups, our method demonstrates consistently strong performance. Its main advantage emerges in challenging settings involving high-dimensional data and large mutual information values. In these regimes, our approach consistently outperforms both the diffusion-based MINDE estimator and classical MI estimation baselines.

5.1 LOW-DIMENSIONAL BENCHMARK

The tests from (Czyż et al., 2023) focus on low-dimensional distributions with tractable mutual information. Various mappings are also applied to make the distributions light- or heavy-tailed, or to non-linearly embed the data into an ambient space of higher dimensionality.

InfoBridge is tested with $\epsilon = 1$ and a multi-layer dense neural network is used to approximate the drifts. Our computational complexity is comparable to MINDE (Franzese et al., 2024). For more details, please, refer to Section D. In each test, we perform 10 independent runs with 100k train set samples and 10k test set samples, where we train *InfoBridge* neural networks for 100k grad steps. We report the mean MI estimation in Tables 1 and 21.

Overall, the performance of our estimator is similar to that of MINDE (§3) and superior to the classical and flow based, methods, with the Cauchy distribution being the only notable exception. Unfortunately, the Cauchy distribution lacks the first moment, which poses theoretical limitations for Bridge Matching (Shi et al., 2023, Appendix C). However, we overcome this limitation using the tail-shortening asinh transform, which enables our method to achieve near-accurate MI estimates, see first two Asinh columns in Tables 1 and 21.

5.2 IMAGE DATA BENCHMARK

In (Butakov et al., 2024b), it was proposed to map low-dimensional distributions with tractable MI into manifolds admitting image-like structure, thus producing synthetic images (in particular, images of 2D Gaussians and Rectangles, see Figures 5a and 5b). By using smooth injective mappings, one ensures that MI is not altered by the transform (Butakov et al., 2024a, Theorem 2.1). In the original works, it is argued that such benchmarks are closer to real data, and therefore closer to realistic setups.

Each neural algorithm is trained with 100k train set samples and validated using 10k samples. In addition we explore experimental setups with less train set samples in Appendix C.3. *InfoBridge* is tested with $\epsilon = 1$, we use a neural network with U-net architecture to approximate the drift and train the model for 100k grad steps with batch size of 64. Other experimental details are reported in Section D.3 and the ablation study on neural network architecture and volatility coefficient ϵ is presented in Section C.2.

Table 2: Mean Absolute Error (MAE) averaged for all setups and random seeds, and standard deviations averaged over setups for Image based benchmark experiment. The best result is **bolded**.

Method	<i>InfoBridge</i>	InfoNCE	KSG	MINE	MIENF	NWJ	MINDE-C	MINDE-J
MAE ↓	0.38	1.44	1.15	0.92	0.45	1.24	0.56	1.66
Average std. ↓	0.07	0.04	0.02	0.13	0.08	0.08	0.43	0.45

We present our results for 16×16 and 32×32 resolution images with both Gaussian and Rectangle structure in Figure 1 and report aggregated MAE and std in Table 2, while the samples from the learned conditional bridge matching models can be viewed in Figures 5c to 5f.

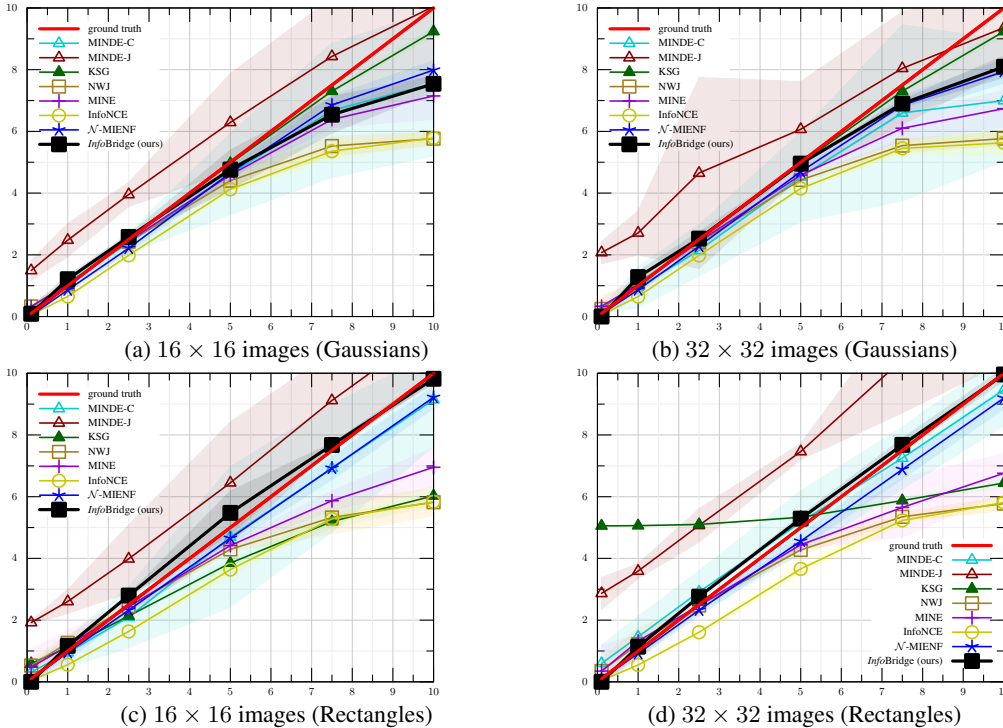


Figure 1: Comparison of the MI estimators. Along x axes is $I(X_0; X_1)$, along y axes is MI estimate $\hat{I}(X_0; X_1)$. We plot 99% confidence intervals acquired from different seed runs.

Our estimator is competitive, being consistently more precise and more stable than both MINDE-C and MINDE-J, and overall slightly better than the previous best-performing method: MIENF (Butakov et al., 2024a). In addition, our method delivers less variance in MI estimation see Table 2.

5.3 PROTEIN EMBEDDINGS DATA

We evaluate *InfoBridge* on real-world data, i.e., conduct experiments on protein language model embeddings. Following the benchmark construction method from (Lee & Rhee, 2024), we generate paired datasets with known MI by ensuring that only class labels are shared between variables X and Y , making the MI analytically tractable (Lee & Rhee, 2024, §4.5). We use sequence embeddings from the ProtTrans5 model (Elnaggar et al., 2021), based on proteins from *A. thaliana* and *H. sapiens*, to create datasets with varying ground truth MI. The final number of training pairs is 20641 and the dimensionality of embeddings is 1024. In addition, the ablation study on the volatility coefficient ϵ is presented in C.2.

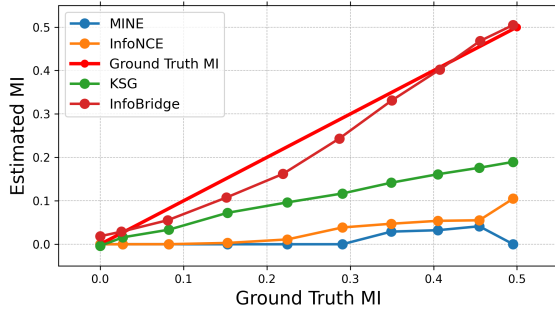


Figure 2: Comparison of the selected estimators on the ProtTrans5 data. Along x axes is ground truth $I(X_0, X_1)$, along y axes is MI estimate $\hat{I}(X_0, X_1)$.

InfoBridge with $\epsilon = 1$ is trained for 100 epochs with batch size of 128 and neural network along the other hyperparameters are similar to the low-dimensional benchmark (§5.1) hyperparameters. We compare against MINE, InfoNCE, KSG, and MINDE. All the technical details can be found in Appendix D.4. We present the results plot in Figure 2 and MAE in Table 14. One can see that *InfoBridge* is the only method to consistently estimate MI accurately; MINDE-C and MINDE-J are omitted as they drastically overestimate MI (e.g., MAE: MINDE-C 9.29 vs. *InfoBridge* 0.04).

5.4 HIGH MUTUAL INFORMATION

‘To evaluate the performance of our method in high mutual information regimes, we conduct experiments on high-dimensional tasks introduced in (Czyż et al., 2023), including correlated uniform, smoothed uniform, correlated gaussian its half cube transformed variant. We systematically vary

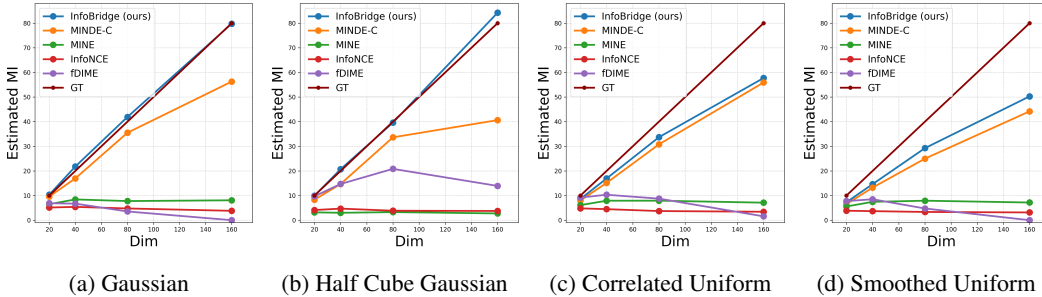


Figure 3: Comparison of MI estimates across dimensions and MI for high mutual information.

the dimensionality and mutual information of the random variables, setting $d \in \{20, 40, 80, 160\}$ and $MI \in \{10, 20, 40, 80\}$. Each experiment uses a training set of 100k samples and a test set of 10k samples. We evaluate our method with $\epsilon = 0.01$ and show the results in Figure 3. The *InfoBridge* is trained for 200 epochs with a batch size of 128, and the neural network is the same as for low-dimensional benchmark § 5.1. To keep the narrative concise, we provide additional baselines and experimental details, refer to Appendix D.5.

As shown, our method yields the most accurate estimates compared to the ground truth, whereas MINE, InfoNCE, and fDIME (GAN, J) fail to capture high mutual information values, and MINDE-C consistently underperforms relative to our approach.

6 DISCUSSION

Potential Impact. Our contributions include the development of novel unbiased estimator for the MI grounded in diffusion bridge matching theory. The proposed algorithm, *InfoBridge*, demonstrates superior performance compared to commonly used MI estimators on both synthetic and real-world challenging high-dimensional benchmarks. Also, our approach can be used to estimate the KL divergence and differential entropy Sections B.1 and B.2.

We believe that our work paves the way for new directions in the estimation of MI *in high dimensions*. This has potential real-world applications such as text-to-image alignment (Wang et al., 2024), self-supervised learning (Bachman et al., 2019), deep neural network analysis (Butakov et al., 2024b), and other use cases in high-dimensional settings.

Moreover, our approach offers opportunities for extension by exploring alternative types of bridges within reciprocal processes, for instance, variance-preserving SDE bridges (Zhou et al., 2024), or by incorporating advanced diffusion bridges techniques like time reweighting (Kim et al., 2025).

7 LIMITATIONS

Bridge Matching as a general generative modeling paradigm is limited w.r.t. distributions without the first moment. To be well defined Bridge Matching procedure requires some assumptions to be satisfied, which are described in Appendix A.1. If one of the $\pi(x_0)$ or $\pi(x_1)$ distributions doesn't have a first moment, then these assumptions are not satisfied, and our method is not guaranteed to work. One such case can be seen in Table 1, one-degree-of-freedom Student-t distribution, i.e., St (dof=1), also known as the Cauchy distribution, that has no first moment.

Acknowledgements. We thank Kirill Sokolov for the careful feedback and support in refining the proofs. The work was supported by the grant for research centers in the field of AI provided by the Ministry of Economic Development of the Russian Federation in accordance with the agreement 000000C313925P4F0002 and the agreement №139-10-2025-033.

LLM Usage. Large Language Models (LLMs) were used only to assist with rephrasing sentences and improving the clarity of the text.

Reproducibility statement. All the technical details that are required to reproduce the work are stated either in main experimental section (§ 5) or Section D. Additionally, we provide code for the reproduction of experiments in supplementary. All the proofs for provided theoretical results are provided either in Section A or Section B.

REFERENCES

- Rana Ali Amjad, Kairen Liu, and Bernhard C. Geiger. Understanding neural networks and individual neuron importance via information-ordered cumulative ablation. *IEEE Transactions on Neural Networks and Learning Systems*, 33(12):7842–7852, 2022. doi: 10.1109/TNNLS.2021.3088685.
- Ziqiao Ao and Jinglai Li. Entropy estimation via normalizing flow. *Proceedings of the AAAI Conference on Artificial Intelligence*, 36(9):9990–9998, Jun. 2022. doi: 10.1609/aaai.v36i9.21237. URL <https://ojs.aaai.org/index.php/AAAI/article/view/21237>.
- Lynton Ardizzone, Radek Mackowiak, Carsten Rother, and Ullrich Köthe. Training normalizing flows with the information bottleneck for competitive generative classification. In H. Larochelle, M. Ranzato, R. Hadsell, M.F. Balcan, and H. Lin (eds.), *Advances in Neural Information Processing Systems*, volume 33, pp. 7828–7840. Curran Associates, Inc., 2020. URL https://proceedings.neurips.cc/paper_files/paper/2020/file/593906af0d138e69f49d251d3e7cbcd0-Paper.pdf.
- Philip Bachman, R Devon Hjelm, and William Buchwalter. Learning representations by maximizing mutual information across views. In H. Wallach, H. Larochelle, A. Beygelzimer, F. d’Alché-Buc, E. Fox, and R. Garnett (eds.), *Advances in Neural Information Processing Systems*, volume 32. Curran Associates, Inc., 2019. URL https://proceedings.neurips.cc/paper_files/paper/2019/file/ddf354219aac374f1d40b7e760ee5bb7-Paper.pdf.
- Mohamed Ishmael Belghazi, Aristide Baratin, Sai Rajeshwar, Sherjil Ozair, Yoshua Bengio, Aaron Courville, and Devon Hjelm. Mutual information neural estimation. In Jennifer Dy and Andreas Krause (eds.), *Proceedings of the 35th International Conference on Machine Learning*, volume 80 of *Proceedings of Machine Learning Research*, pp. 531–540. PMLR, 07 2018. URL <https://proceedings.mlr.press/v80/belghazi18a.html>.
- A J Bell and T J Sejnowski. An information-maximization approach to blind separation and blind deconvolution. *Neural Comput.*, 7(6):1129–1159, November 1995.
- Thomas Berrett and Richard Samworth. Nonparametric independence testing via mutual information. *Biometrika*, 106, 11 2017. doi: 10.1093/biomet/asz024.
- Thomas B. Berrett, Richard J. Samworth, and Ming Yuan. Efficient multivariate entropy estimation via k -nearest neighbour distances. *Ann. Statist.*, 47(1):288–318, 02 2019. doi: 10.1214/18-AOS1688. URL <https://doi.org/10.1214/18-AOS1688>.
- Valentin De Bortoli, Iryna Korshunova, Andriy Mnih, and Arnaud Doucet. Schrodinger bridge flow for unpaired data translation. In *The Thirty-eighth Annual Conference on Neural Information Processing Systems*, 2024. URL <https://openreview.net/forum?id=1F32iCJFfa>.
- Mustapha Bounoua, Giulio Franzese, and Pietro Michiardi. \mathcal{S}_{wi} : Score-based o-INFORMATION estimation. In Ruslan Salakhutdinov, Zico Kolter, Katherine Heller, Adrian Weller, Nuria Oliver, Jonathan Scarlett, and Felix Berkenkamp (eds.), *Proceedings of the 41st International Conference on Machine Learning*, volume 235 of *Proceedings of Machine Learning Research*, pp. 4444–4471. PMLR, 21–27 Jul 2024a. URL <https://proceedings.mlr.press/v235/bounoua24a.html>.
- Mustapha Bounoua, Giulio Franzese, and Pietro Michiardi. \mathcal{S}_{wi} : Score-based o-information estimation. In *ICML 2024, 41st International Conference on Machine Learning*, 2024b.
- Charlotte Bunne, Ya-Ping Hsieh, Marco Cuturi, and Andreas Krause. The schrödinger bridge between gaussian measures has a closed form. In *International Conference on Artificial Intelligence and Statistics*, pp. 5802–5833. PMLR, 2023.
- Ivan Butakov, Alexander Tolmachev, Sofia Malanchuk, Anna Neopryatnaya, and Alexey Frolov. Mutual information estimation via normalizing flows. In *The Thirty-eighth Annual Conference on Neural Information Processing Systems*, 2024a. URL <https://openreview.net/forum?id=JiQXsLvDls>.

- Ivan Butakov, Alexander Tolmachev, Sofia Malanchuk, Anna Neopryatnaya, Alexey Frolov, and Kirill Andreev. Information bottleneck analysis of deep neural networks via lossy compression. In *The Twelfth International Conference on Learning Representations*, 2024b. URL <https://openreview.net/forum?id=huGECz8dPp>.
- Xavier Aramayo Carrasco, Grigoriy Ksenofontov, Aleksei Leonov, Iaroslav Sergeevich Koshelev, and Alexander Korotin. Entering the era of discrete diffusion models: A benchmark for schrödinger bridges and entropic optimal transport. In *The Fourteenth International Conference on Learning Representations*, 2026. URL <https://openreview.net/forum?id=XcPDT615Gd>.
- Xi Chen, Yan Duan, Rein Houthooft, John Schulman, Ilya Sutskever, and Pieter Abbeel. Info-gan: Interpretable representation learning by information maximizing generative adversarial nets. In Daniel D. Lee, Masashi Sugiyama, Ulrike von Luxburg, Isabelle Guyon, and Roman Garnett (eds.), *Advances in Neural Information Processing Systems 29: Annual Conference on Neural Information Processing Systems 2016, December 5-10, 2016, Barcelona, Spain*, pp. 2172–2180, 2016. URL <https://proceedings.neurips.cc/paper/2016/hash/7c9d0b1f96aebd7b5eca8c3edaa19ebb-Abstract.html>.
- Zehua Chen, Guande He, Kaiwen Zheng, Xu Tan, and Jun Zhu. Schrodinger bridges beat diffusion models on text-to-speech synthesis. *arXiv preprint arXiv:2312.03491*, 2023.
- Thomas M. Cover and Joy A. Thomas. *Elements of Information Theory (Wiley Series in Telecommunications and Signal Processing)*. Wiley-Interscience, USA, 2006.
- Paweł Czyż, Frederic Grabowski, Julia E Vogt, Niko Beerenwinkel, and Alexander Marx. Beyond normal: On the evaluation of mutual information estimators. In *Thirty-seventh Conference on Neural Information Processing Systems*, 2023. URL <https://openreview.net/forum?id=25vRtG56YH>.
- Caleb Dahlke and Jason Pacheco. Flow-based variational mutual information: Fast and flexible approximations. In *The Thirteenth International Conference on Learning Representations*, 2025.
- Valentin De Bortoli, Guan-Horng Liu, Tianrong Chen, Evangelos A Theodorou, and Weilie Nie. Augmented bridge matching. *arXiv preprint arXiv:2311.06978*, 2023.
- J. L. Doob. Conditional brownian motion and the boundary limits of harmonic functions. *Bulletin de la Société Mathématique de France*, 85:431–458, 1957.
- Giovanni Dosi and Andrea Roventini. More is different... and complex! the case for agent-based macroeconomics. *Journal of Evolutionary Economics*, 29:1–37, 2019.
- Bao Duong and Thin Nguyen. Diffeomorphic information neural estimation. *Proceedings of the AAAI Conference on Artificial Intelligence*, 37(6):7468–7475, Jun. 2023a. doi: 10.1609/aaai.v37i6.25908. URL <https://ojs.aaai.org/index.php/AAAI/article/view/25908>.
- Bao Duong and Thin Nguyen. Normalizing flows for conditional independence testing. *Knowledge and Information Systems*, 66, 08 2023b. doi: 10.1007/s10115-023-01964-w.
- Ahmed Elnaggar, Michael Heinzinger, Christian Dallago, Ghalia Rehawi, Yu Wang, Llion Jones, Tom Gibbs, Tamas Feher, Christoph Angerer, Martin Steinegger, et al. Prottrans: towards cracking the language of life’s code through self-supervised learning. *IEEE Transactions on Pattern Analysis and Machine Intelligence*, 44:7112–7127, 2021.
- Ammar Fayad and Majd Ibrahim. On slicing optimality for mutual information. In *Thirty-seventh Conference on Neural Information Processing Systems*, 2023. URL <https://openreview.net/forum?id=JMufZx2xU>.
- Marco Federici, David Ruhe, and Patrick Forré. On the effectiveness of hybrid mutual information estimation, 2023. URL <https://arxiv.org/abs/2306.00608>.
- Giulio Franzese, Mustapha BOUNOUA, and Pietro Michiardi. MINDE: Mutual information neural diffusion estimation. In *The Twelfth International Conference on Learning Representations*, 2024. URL <https://openreview.net/forum?id=0kWd8SJq8d>.

- Z. Goldfeld, K. Greenewald, J. Niles-Weed, and Y. Polyanskiy. Convergence of smoothed empirical measures with applications to entropy estimation. *IEEE Transactions on Information Theory*, 66(7):4368–4391, 2020. doi: 10.1109/TIT.2020.2975480.
- Ziv Goldfeld and Kristjan Greenewald. Sliced mutual information: A scalable measure of statistical dependence. In A. Beygelzimer, Y. Dauphin, P. Liang, and J. Wortman Vaughan (eds.), *Advances in Neural Information Processing Systems*, 2021. URL <https://openreview.net/forum?id=SvrY1-FDq2>.
- Ziv Goldfeld, Ewout van den Berg, Kristjan H. Greenewald, Igor V. Melnyk, Nam H. Nguyen, Brian Kingsbury, and Yuri Polyanskiy. Estimating information flow in deep neural networks. In *ICML*, 2019.
- Ziv Goldfeld, Kristjan Greenewald, Theshani Nuradha, and Galen Reeves. \mathbb{S} -sliced mutual information: A quantitative study of scalability with dimension. In Alice H. Oh, Alekh Agarwal, Danielle Belgrave, and Kyunghyun Cho (eds.), *Advances in Neural Information Processing Systems*, 2022. URL <https://openreview.net/forum?id=L-ceBdl2DPb>.
- Kristjan H. Greenewald, Brian Kingsbury, and Yuancheng Yu. High-dimensional smoothed entropy estimation via dimensionality reduction. In *IEEE International Symposium on Information Theory, ISIT 2023, Taipei, Taiwan, June 25-30, 2023*, pp. 2613–2618. IEEE, 2023. doi: 10.1109/ISIT54713.2023.10206641. URL <https://doi.org/10.1109/ISIT54713.2023.10206641>.
- Nikita Gushchin, Alexander Kolesov, Alexander Korotin, Dmitry Vetrov, and Evgeny Burnaev. Entropic neural optimal transport via diffusion processes. In *Advances in Neural Information Processing Systems*, 2023a.
- Nikita Gushchin, Alexander Kolesov, Petr Mokrov, Polina Karpikova, Andrey Spiridonov, Evgeny Burnaev, and Alexander Korotin. Building the bridge of schrödinger: A continuous entropic optimal transport benchmark. In *Thirty-seventh Conference on Neural Information Processing Systems Datasets and Benchmarks Track*, 2023b.
- Nikita Gushchin, Sergei Kholkin, Evgeny Burnaev, and Alexander Korotin. Light and optimal schrödinger bridge matching. In *Forty-first International Conference on Machine Learning*, 2024a.
- Nikita Gushchin, Daniil Selikhanovych, Sergei Kholkin, Evgeny Burnaev, and Alexander Korotin. Adversarial schrödinger bridge matching. *Advances in Neural Information Processing Systems*, 37: 89612–89651, 2024b.
- Nikita Gushchin, David Li, Daniil Selikhanovych, Evgeny Burnaev, Dmitry Baranchuk, and Alexander Korotin. Inverse bridge matching distillation. In *International Conference on Machine Learning*, pp. 21471–21496. PMLR, 2025.
- Guande He, Kaiwen Zheng, Jianfei Chen, Fan Bao, and Jun Zhu. Consistency diffusion bridge models. *Advances in Neural Information Processing Systems*, 37:23516–23548, 2024.
- R Devon Hjelm, Alex Fedorov, Samuel Lavoie-Marchildon, Karan Grewal, Phil Bachman, Adam Trischler, and Yoshua Bengio. Learning deep representations by mutual information estimation and maximization. In *International Conference on Learning Representations*, 2019. URL <https://openreview.net/forum?id=Bklr3j0cKX>.
- Jonathan Ho and Tim Salimans. Classifier-free diffusion guidance. In *NeurIPS 2021 Workshop on Deep Generative Models and Downstream Applications*, 2021.
- Jonathan Ho, Ajay Jain, and Pieter Abbeel. Denoising diffusion probabilistic models. *Advances in Neural Information Processing Systems*, 33:6840–6851, 2020.
- Oliver Ibe. *Markov processes for stochastic modeling*. Newnes, 2013.
- Iliia Igashov, Arne Schneuing, Marwin Segler, Michael M Bronstein, and Bruno Correia. Retrobridge: Modeling retrosynthesis with markov bridges. In *The Twelfth International Conference on Learning Representations*, 2024.
- Bert Kappen. Lecture notes in cds machine learning, September 2024.

- Sergei Kholkin, Grigoriy Ksenofontov, David Li, Nikita Kornilov, Nikita Gushchin, Alexandra Suvorikova, Alexey Kroshnin, Evgeny Burnaev, and Alexander Korotin. Diffusion & adversarial schrödinger bridges via iterative proportional markovian fitting. In *The Fourteenth International Conference on Learning Representations*, 2026. URL <https://openreview.net/forum?id=38fGCBhFF5>.
- Beomsu Kim, Yu-Guan Hsieh, Michal Klein, Marco Cuturi, Jong Chul Ye, Bahjat Kawar, and James Thornton. Simple reflow: Improved techniques for fast flow models. In *The Thirteenth International Conference on Learning Representations*, 2025. URL <https://openreview.net/forum?id=fpvgSDKXGY>.
- Diederik P. Kingma and Jimmy Ba. Adam: A method for stochastic optimization, 2017.
- Durk P Kingma and Prafulla Dhariwal. Glow: Generative flow with invertible 1x1 convolutions. *Advances in neural information processing systems*, 31, 2018.
- Alexander Korotin, Nikita Gushchin, and Evgeny Burnaev. Light schrödinger bridge. In *The Twelfth International Conference on Learning Representations*, 2024.
- L. F. Kozachenko and N. N. Leonenko. Sample estimate of the entropy of a random vector. *Problems Inform. Transmission*, 23:95–101, 1987.
- Alexander Kraskov, Harald Stögbauer, and Peter Grassberger. Estimating mutual information. *Phys. Rev. E*, 69:066138, Jun 2004. doi: 10.1103/PhysRevE.69.066138. URL <https://link.aps.org/doi/10.1103/PhysRevE.69.066138>.
- Grigoriy Ksenofontov and Alexander Korotin. Categorical schrödinger bridge matching. In *International Conference on Machine Learning*, pp. 31727–31751. PMLR, 2025.
- Kyungeun Lee and Wonjong Rhee. A benchmark suite for evaluating neural mutual information estimators on unstructured datasets. *Advances in Neural Information Processing Systems*, 37: 46319–46338, 2024.
- Christian Léonard. Girsanov theory under a finite entropy condition. In Catherine Donati-Martin, Antoine Lejay, and Alain Rouault (eds.), *Séminaire de Probabilités XLIV*, volume 2046 of *Lecture Notes in Mathematics*, pp. 429–465. Springer, Berlin, Heidelberg, 2012.
- Christian Léonard. Stochastic derivatives and generalized h-transforms of markov processes, 2013.
- Christian Léonard. A survey of the Schrödinger problem and some of its connections with optimal transport. *Discrete and Continuous Dynamical Systems - Series A*, 34(4):1533–1574, 2014a.
- Christian Léonard. Some properties of path measures. *Séminaire de Probabilités XLVI*, pp. 207–230, 2014b.
- Christian Léonard, Sylvie Roelly, and Jean-Claude Zambrini. Reciprocal processes. a measure-theoretical point of view. *Probability Surveys*, 11:237–269, 2014.
- Nunzio Alexandro Letizia, Nicola Novello, and Andrea M Tonello. Mutual information estimation via f -divergence and data derangements. *Advances in Neural Information Processing Systems*, 37: 105114–105150, 2024.
- R. Linsker. Self-organization in a perceptual network. *Computer*, 21(3):105–117, 1988. doi: 10.1109/2.36.
- Guan-Horng Liu, Arash Vahdat, De-An Huang, Evangelos A Theodorou, Weili Nie, and Anima Anandkumar. I²sb: Image-to-image schrödinger bridge. *arXiv preprint arXiv:2302.05872*, 2023.
- David McAllester and Karl Stratos. Formal limitations on the measurement of mutual information. In Silvia Chiappa and Roberto Calandra (eds.), *Proceedings of the Twenty Third International Conference on Artificial Intelligence and Statistics*, volume 108 of *Proceedings of Machine Learning Research*, pp. 875–884. PMLR, 08 2020. URL <https://proceedings.mlr.press/v108/mcallester20a.html>.

- XuanLong Nguyen, Martin J Wainwright, and Michael I Jordan. Estimating divergence functionals and the likelihood ratio by convex risk minimization. *IEEE Transactions on Information Theory*, 56(11):5847–5861, 2010.
- Bernt Øksendal. *Stochastic differential equations*. Springer, 2003.
- Zbigniew Palmowski and Tomasz Rolski. A technique for exponential change of measure for markov processes. *Bernoulli*, pp. 767–785, 2002.
- Stefano Peluchetti. Diffusion bridge mixture transports, schrödinger bridge problems and generative modeling. *Journal of Machine Learning Research*, 24(374):1–51, 2023.
- Y. Polyanskiy and Y. Wu. *Information Theory: From Coding to Learning*. Cambridge University Press, 2024. ISBN 9781108832908. URL <https://books.google.ru/books?id=CySo0AEACAAJ>.
- Benjamin Rhodes, Kai Xu, and Michael U. Gutmann. Telescoping density-ratio estimation. In H. Larochelle, M. Ranzato, R. Hadsell, M.F. Balcan, and H. Lin (eds.), *Advances in Neural Information Processing Systems*, volume 33, pp. 4905–4916. Curran Associates, Inc., 2020. URL https://proceedings.neurips.cc/paper_files/paper/2020/file/33d3b157ddc0896addfb22fa2a519097-Paper.pdf.
- Robin Rombach, Andreas Blattmann, Dominik Lorenz, Patrick Esser, and Björn Ommer. High-resolution image synthesis with latent diffusion models. In *Proceedings of the IEEE/CVF Conference on Computer Vision and Pattern Recognition*, pp. 10684–10695, 2022.
- Olaf Ronneberger, Philipp Fischer, and Thomas Brox. U-net: Convolutional networks for biomedical image segmentation. In *Medical image computing and computer-assisted intervention—MICCAI 2015: 18th international conference, Munich, Germany, October 5-9, 2015, proceedings, part III 18*, pp. 234–241. Springer, 2015.
- Fernando E Rosas, Pedro AM Mediano, Michael Gastpar, and Henrik J Jensen. Quantifying high-order interdependencies via multivariate extensions of the mutual information. *Physical Review E*, 100(3):032305, 2019.
- Jakob Runge, Sebastian Bathiany, Erik Bollt, Gustau Camps-Valls, Dim Coumou, Ethan Deyle, Clark Glymour, Marlene Kretschmer, Miguel D Mahecha, Jordi Muñoz-Marí, et al. Inferring causation from time series in earth system sciences. *Nature communications*, 10(1):2553, 2019.
- Erwin Schrödinger. Sur la théorie relativiste de l’électron et l’interprétation de la mécanique quantique. In *Annales de l’institut Henri Poincaré*, volume 2, pp. 269–310, 1932.
- Rajat Sen, Ananda Theertha Suresh, Karthikeyan Shanmugam, Alexandros G Dimakis, and Sanjay Shakkottai. Model-powered conditional independence test. In I. Guyon, U. Von Luxburg, S. Bengio, H. Wallach, R. Fergus, S. Vishwanathan, and R. Garnett (eds.), *Advances in Neural Information Processing Systems*, volume 30. Curran Associates, Inc., 2017. URL https://proceedings.neurips.cc/paper_files/paper/2017/file/02f039058bd48307e6f653a2005c9dd2-Paper.pdf.
- Yuyang Shi, Valentin De Bortoli, Andrew Campbell, and Arnaud Doucet. Diffusion schrödinger bridge matching. In *Thirty-seventh Conference on Neural Information Processing Systems*, 2023. URL <https://openreview.net/forum?id=qy07OHsJT5>.
- Vignesh Ram Somnath, Matteo Pariset, Ya-Ping Hsieh, Maria Rodriguez Martinez, Andreas Krause, and Charlotte Bunne. Aligned diffusion schrödinger bridges. In *Uncertainty in Artificial Intelligence*, pp. 1985–1995. PMLR, 2023.
- Jiaming Song and Stefano Ermon. Understanding the limitations of variational mutual information estimators. In *International Conference on Learning Representations*, 2020. URL <https://openreview.net/forum?id=B1x62TNtDS>.
- Yang Song, Jascha Sohl-Dickstein, Diederik P Kingma, Abhishek Kumar, Stefano Ermon, and Ben Poole. Score-based generative modeling through stochastic differential equations. In *International Conference on Learning Representations*, 2021.

- Thomas Steinke and Lydia Zakyntinou. Reasoning About Generalization via Conditional Mutual Information. In Jacob Abernethy and Shivani Agarwal (eds.), *Proceedings of Thirty Third Conference on Learning Theory*, volume 125 of *Proceedings of Machine Learning Research*, pp. 3437–3452. PMLR, 09–12 Jul 2020. URL <https://proceedings.mlr.press/v125/steinke20a.html>.
- Vincent Stimper, David Liu, Andrew Campbell, Vincent Berenz, Lukas Ryll, Bernhard Schölkopf, and José Miguel Hernández-Lobato. normflows: A pytorch package for normalizing flows. *Journal of Open Source Software*, 8(86):5361, 2023. doi: 10.21105/joss.05361. URL <https://doi.org/10.21105/joss.05361>.
- Karl Stratos. Mutual information maximization for simple and accurate part-of-speech induction. In Jill Burstein, Christy Doran, and Thamar Solorio (eds.), *Proceedings of the 2019 Conference of the North American Chapter of the Association for Computational Linguistics: Human Language Technologies, Volume 1 (Long and Short Papers)*, pp. 1095–1104, Minneapolis, Minnesota, June 2019. Association for Computational Linguistics. doi: 10.18653/v1/N19-1113. URL <https://aclanthology.org/N19-1113/>.
- Naftali Tishby and Noga Zaslavsky. Deep learning and the information bottleneck principle. *2015 IEEE Information Theory Workshop (ITW)*, pp. 1–5, 2015.
- Alexander Y Tong, Nikolay Malkin, Kilian Fatras, Lazar Atanackovic, Yanlei Zhang, Guillaume Huguet, Guy Wolf, and Yoshua Bengio. Simulation-free schrödinger bridges via score and flow matching. In *International Conference on Artificial Intelligence and Statistics*, pp. 1279–1287. PMLR, 2024.
- Michael Tschannen, Josip Djolonga, Paul K. Rubenstein, Sylvain Gelly, and Mario Lucic. On mutual information maximization for representation learning. In *International Conference on Learning Representations*, 2020. URL <https://openreview.net/forum?id=rkxoh24FPH>.
- Dor Tsur, Ziv Goldfeld, and Kristjan Greenewald. Max-sliced mutual information. In *Thirty-seventh Conference on Neural Information Processing Systems*, 2023. URL <https://openreview.net/forum?id=ce9B2x3zQa>.
- Aaron van den Oord, Yazhe Li, and Oriol Vinyals. Representation learning with contrastive predictive coding, 2019. URL <https://arxiv.org/abs/1807.03748>.
- Francisco Vargas, Pierre Thodoroff, Austen Lamacraft, and Neil Lawrence. Solving schrödinger bridges via maximum likelihood. *Entropy*, 23(9):1134, 2021.
- Francisco Vargas, Andrius Ovsianas, David Fernandes, Mark Girolami, Neil D Lawrence, and Nikolas Nüsken. Bayesian learning via neural schrödinger–föllmer flows. *Statistics and Computing*, 33(1): 3, 2023.
- Petar Veličković, William Fedus, William L. Hamilton, Pietro Liò, Yoshua Bengio, and R Devon Hjelm. Deep graph infomax. In *International Conference on Learning Representations*, 2019. URL <https://openreview.net/forum?id=rklz9iAcKQ>.
- Chao Wang, Giulio Franzese, Alessandro Finamore, Massimo Gallo, and Pietro Michiardi. Information theoretic text-to-image alignment, 2024. URL <https://arxiv.org/abs/2405.20759>.
- Stanislaw Węglarczyk. Kernel density estimation and its application. *ITM Web of Conferences*, 23: 00037, 01 2018. doi: 10.1051/itmconf/20182300037.
- Aolin Xu and Maxim Raginsky. Information-theoretic analysis of generalization capability of learning algorithms. *Advances in neural information processing systems*, 30, 2017.
- Linqi Zhou, Aaron Lou, Samar Khanna, and Stefano Ermon. Denoising diffusion bridge models. In *The Twelfth International Conference on Learning Representations*, 2024.

APPENDIX CONTENTS

A Proofs	17
A.1 Auxiliary results	17
A.2 Proof of Theorem 4.1	20
B Extensions of our methodology	21
B.1 KL divergence estimator	21
B.2 Differential entropy estimator	22
B.3 Entropy estimation experiments	22
B.4 Interaction information	23
B.5 Mutual Information between random variables of different dimensionality	23
C Additional discussion on method	24
C.1 Conceptual comparison with MINDE	24
C.2 Ablation study	24
C.3 Train sample size study	26
C.4 Strategies for drawing train samples	26
C.5 One neural network approach versus two neural networks approach	27
D Experimental supplementary	27
D.1 Metrics	27
D.2 Low-dimensional benchmark	28
D.3 Image data benchmark	28
D.4 Protein embeddings data	31
D.5 High mutual information experiments	33

A PROOFS

A.1 AUXILIARY RESULTS

The following subsection mostly contains results very similar to the ones presented in (Doob, 1957) and the comprehensive derivations are presented for the reader convenience.

Setup Let $\Omega = C([0, 1], \mathbb{R}^D)$, $X_t(\omega) = \omega(t)$, $\mathcal{F}_t = \sigma(X_s : s \leq t)$. Let $\pi \in \mathbb{P}(\mathbb{R}^D \times \mathbb{R}^D)$ with marginals π_0, π_1 . Let P^{x_0} be Brownian motion with volatility $\sqrt{\varepsilon}$ started at x_0 . Its transition density is

$$p_t^\varepsilon(x, y) = (2\pi\varepsilon t)^{-D/2} \exp\left(-\frac{\|y - x\|^2}{2\varepsilon t}\right).$$

We fix a regular version of the Brownian bridge kernel $W_{|x_0, x_1}^\varepsilon$ which is measurable.

$$Q_\pi := \int W_{|x_0, x_1}^\varepsilon d\pi(x_0, x_1),$$

Let $\mu^{x_0} := \pi(\cdot|x_0)$. For $t \in (0, 1)$ define the h -functions:

$$h^{x_0}(t, x) := \int_{\mathbb{R}^D} \frac{p_{1-t}^\varepsilon(x, y)}{p_1^\varepsilon(x_0, y)} d\mu^{x_0}(y).$$

Intuitively, $h^{x_0}(t, x)$ is the likelihood factor that reweights the reference Brownian motion started at x_0 so that, at final time 1, it has terminal law μ^{x_0} .

Assumption A.1. $\int_{\mathbb{R}^D} \|x_1\| d\pi_1(x_1) < \infty$.

Lemma A.2. Fix $\delta \in (0, 1/2)$ and $x_0 \in \mathbb{R}^D$. Then:

1. $h_\pi^{x_0}(t, x) \in (0, \infty)$ for all $(t, x) \in [\delta, 1 - \delta] \times \mathbb{R}^D$;
2. $h_\pi^{x_0} \in C^{1,2}([\delta, 1 - \delta] \times \mathbb{R}^D)$;
3. on each compact $K \subset \mathbb{R}^D$, $\inf_{[\delta, 1 - \delta] \times K} h_\pi^{x_0} > 0$ and $\nabla_x \log h_\pi^{x_0}$ is Lipschitz in x on $[\delta, 1 - \delta] \times K$.

Proof. Set

$$K_{t,x,x_0}(y) := \frac{p_{1-t}^\varepsilon(x, y)}{p_1^\varepsilon(x_0, y)}.$$

A direct computation shows that, for each fixed $t \in (0, 1)$,

$$K_{t,x,x_0}(y) = C(t) \exp\left(-\frac{t}{2\varepsilon(1-t)}\|y\|^2 + b(t, x, x_0) \cdot y + c(t, x, x_0)\right),$$

where $C(t) = (1-t)^{-D/2}$ and b, c are affine/quadratic expressions in x, x_0 (their exact form is not important). Crucially, the coefficient in front of $\|y\|^2$ is *negative* and bounded away from 0 when $t \in [\delta, 1 - \delta]$. Therefore, for such t the function $y \mapsto K_{t,x,x_0}(y)$ is strictly positive and achieves a finite maximum, hence is bounded.

(1) Positivity and finiteness. Since $K_{t,x,x_0}(y) > 0$ and bounded in y for each fixed (t, x) with $t \in [\delta, 1 - \delta]$, integrating against the probability measure μ^{x_0} gives $0 < h_\pi^{x_0}(t, x) < \infty$.

(2) $C^{1,2}$ regularity. For $|\alpha| \leq 2$, the derivatives $\partial_x^\alpha K_{t,x,x_0}(y)$ are polynomials in y times the same exponential factor, hence they are also bounded in y for $t \in [\delta, 1 - \delta]$. Thus, on any set $[\delta, 1 - \delta] \times \{x\}$ we can differentiate under the integral sign by dominated convergence, obtaining that $h_\pi^{x_0}$ is $C^{1,2}$ in (t, x) .

(3) Positive lower bound and Lipschitzness of $\nabla \log h$ on compacts. Fix a compact $K \subset \mathbb{R}^D$. Continuity of h^{x_0} on the compact set $[\delta, 1 - \delta] \times K$ implies it attains its minimum there; by (1) this minimum is positive, so $m := \inf_{[\delta, 1 - \delta] \times K} h^{x_0} > 0$.

Moreover, by (2) the derivatives ∇h and $\nabla^2 h$ are continuous, hence bounded on $[\delta, 1 - \delta] \times K$. Finally, using $\nabla \log h = (\nabla h)/h$ and the identity

$$\nabla^2 \log h = \frac{\nabla^2 h}{h} - \frac{\nabla h \otimes \nabla h}{h^2},$$

we see that $\nabla^2 \log h$ is bounded on $[\delta, 1 - \delta] \times K$. A bounded Hessian implies that $\nabla \log h$ is Lipschitz in x on this set. \square

Proposition A.3. For each x_0 and each $t < 1$, the conditional laws

$$Q_\pi^{x_0} := Q_\pi(\cdot|X_0 = x_0),$$

satisfy, for any $A \in \mathcal{F}_t$,

$$Q_\pi^{x_0}(A) = \mathbb{E}_{P^{x_0}}[\mathbf{1}_A h_\pi^{x_0}(t, X_t)].$$

Consequently, on every interval $[\delta, 1 - \delta]$ the process under $Q_\pi^{x_0}$ solves the SDE (weakly)

$$dX_t = v_\pi^{x_0}(t, X_t) dt + \sqrt{\varepsilon} dW_t, \quad v_\pi^{x_0}(t, x) := \varepsilon \nabla_x \log h_\pi^{x_0}(t, x),$$

and $v_\pi^{x_0}$ is locally Lipschitz in x there.

Proof. Let $A \in \mathcal{F}_t$. By the Markov property of Brownian motion,

$$\mathbb{P}^{x_0}(A, X_1 \in dy) = \mathbb{E}_{P^{x_0}}[\mathbf{1}_A p_{1-t}^\varepsilon(X_t, y)] dy,$$

and also $\mathbb{P}^{x_0}(X_1 \in dy) = p_1^\varepsilon(x_0, y) dy$. Therefore, by Bayes' rule (i.e. by the definition of a regular conditional distribution),

$$W_{|x_0, y}^\varepsilon(A) = \mathbb{P}^{x_0}(A | X_1 = y) = \frac{\mathbb{E}_{P^{x_0}}[\mathbf{1}_A p_{1-t}^\varepsilon(X_t, y)]}{p_1^\varepsilon(x_0, y)}.$$

Now integrate the previous identity in y against $\mu_\pi^{x_0}(dy)$. Since $A \in \mathcal{F}_t$, we can pull $\mathbf{1}_A$ outside the y -integral:

$$\begin{aligned} Q_\pi^{x_0}(A) &= \int W_{|x_0, y}^\varepsilon(A) \mu_\pi^{x_0}(dy) = \\ &= \mathbb{E}_{P^{x_0}}\left[\mathbf{1}_A \int \frac{p_{1-t}^\varepsilon(X_t, y)}{p_1^\varepsilon(x_0, y)} \mu_\pi^{x_0}(dy)\right] = \mathbb{E}_{P^{x_0}}[\mathbf{1}_A h_\pi^{x_0}(t, X_t)]. \end{aligned}$$

In other words, on \mathcal{F}_t the measure $Q_\pi^{x_0}$ is absolutely continuous w.r.t. P^{x_0} with Radon–Nikodym derivative $h_\pi^{x_0}(t, X_t)$ (Doob, 1957; Léonard, 2014a).

On $[\delta, 1 - \delta]$ Lemma A.2 gives that $h_\pi^{x_0}$ is strictly positive and $C^{1,2}$. Moreover, $x \mapsto p_{1-t}^\varepsilon(x, y)$ solves the heat equation, hence $(t, x) \mapsto h_\pi^{x_0}(t, x)$ solves the backward heat equation on $t < 1$.

Let $L := \frac{\varepsilon}{2} \Delta$ be generator under P^{x_0} . Since $(\partial_t + L)h_\pi^{x_0} = 0$ on $t < 1$, Itô's formula gives, for $t \leq 1 - \delta$,

$$dh_\pi^{x_0}(t, X_t) = \nabla h_\pi^{x_0}(t, X_t) \cdot \sqrt{\varepsilon} dW_t = h_\pi^{x_0}(t, X_t) \sqrt{\varepsilon} \nabla \log h_\pi^{x_0}(t, X_t) \cdot dW_t.$$

Hence $M_t := h_\pi^{x_0}(t, X_t)$ is a positive P^{x_0} -martingale and $dM_t = M_t \theta_t \cdot dW_t$ with $\theta_t := \sqrt{\varepsilon} \nabla \log h_\pi^{x_0}(t, X_t)$. Define Q on \mathcal{F}_t by $dQ|_{\mathcal{F}_t} = M_t dP^{x_0}|_{\mathcal{F}_t}$; then by Girsanov,

$$W_t^Q := W_t - \int_0^t \theta_s ds$$

is a Brownian motion under Q , and therefore

$$dX_t = \sqrt{\varepsilon} dW_t = \varepsilon \nabla \log h_\pi^{x_0}(t, X_t) dt + \sqrt{\varepsilon} dW_t^Q.$$

Consequently the generator under Q is $L^Q f = \frac{\varepsilon}{2} \Delta f + \varepsilon \nabla \log h_\pi^{x_0} \cdot \nabla f$, i.e. the claimed SDE with drift $v_\pi^{x_0} = \varepsilon \nabla \log h_\pi^{x_0}$ (Léonard, 2013; 2014a).

Local Lipschitzness on compacts follows from Lemma A.2. \square

Lemma A.4. *Assume A.1. Then for each fixed x_0 and each $t \in (0, 1)$,*

$$v_\pi^{x_0}(t, x) = \mathbb{E}_{Q_\pi^{x_0}}\left[\frac{X_1 - x}{1 - t} \mid X_t = x\right].$$

Proof. Under $Q_\pi^{x_0}$ we first draw $X_1 \sim \mu_\pi^{x_0}$ and then, conditional on $X_1 = y$, run the Brownian bridge from x_0 to y . Hence, for fixed $t < 1$ and $X_t = x$, the conditional distribution of X_1 is proportional to

$$y \mapsto \frac{p_{1-t}^\varepsilon(x, y)}{p_1^\varepsilon(x_0, y)} d\mu_\pi^{x_0}(y).$$

Assumption A.1 implies $\int \|y\| d\pi_1(y) < \infty$, and therefore $\mathbb{E}\|X_1\| < \infty$ under π_1 . For π , note that $\mathbb{E}_\pi\|X_1\|^2 = \mathbb{E}_{\pi_1}\|y\|^2 < \infty$, hence $\mathbb{E}[\|X_1\|^2 | X_0] < \infty$ π_0 -a.s., so $\mu_\pi^{x_0}$ has finite second moment for π_0 -a.e. x_0 and the conditional mean is finite.

Differentiate

$$h_\pi^{x_0}(t, x) = \int \frac{p_{1-t}^\varepsilon(x, y)}{p_1^\varepsilon(x_0, y)} d\mu_\pi^{x_0}(y)$$

with respect to x (justified for any fixed $t > 0$ exactly as in Lemma A.2). Using the Gaussian identity

$$\varepsilon \nabla_x p_{1-t}^\varepsilon(x, y) = \frac{y-x}{1-t} p_{1-t}^\varepsilon(x, y),$$

we obtain

$$\varepsilon \nabla_x h_\pi^{x_0}(t, x) = \int \frac{y-x}{1-t} \frac{p_{1-t}^\varepsilon(x, y)}{p_{1-t}^\varepsilon(x_0, y)} d\mu_\pi^{x_0}(y).$$

Now divide both sides by $h_\pi^{x_0}(t, x)$. Since the conditional law of X_1 given $X_t = x$ has density proportional to the same integrand, the right-hand side is exactly the conditional expectation of $(X_1 - x)/(1-t)$. Therefore,

$$v_\pi^{x_0}(t, x) = \varepsilon \nabla_x \log h_\pi^{x_0}(t, x) = \mathbb{E}_{Q_\pi^{x_0}} \left[\frac{X_1 - x}{1-t} \mid X_t = x \right].$$

□

A.2 PROOF OF THEOREM 4.1

Proof. Using the disintegration theorem and additive property of relative entropy (Léonard, 2014b, Theorems 1.6, 2.4) at time $t = 0$, we get:

$$\text{KL}(Q_\pi \| Q_\pi^{\text{ind}}) = \text{KL}(\pi(x_0) \| \pi(x_0)) + \mathbb{E}_{\pi(x_0)} [\text{KL}(Q_{\pi|x_0} \| Q_{\pi|x_0}^{\text{ind}})].$$

Note that since $Q_\pi, Q_\pi^{\text{ind}}$ share the same marginals at time $t = 0$, first KL term vanishes. In addition, $\text{KL}(Q_{\pi|x_0} \| Q_{\pi|x_0}^{\text{ind}}) < \infty$ for π_0 -a.e. x_0 , since the $I(X_0; X_1) < \infty$. Similarly, by using the disintegration theorem again for both times $t = 0, 1$, we get:

$$\text{KL}(Q_\pi \| Q_\pi^{\text{ind}}) = \text{KL}(\pi(x_0, x_1) \| \pi(x_0)\pi(x_1)) + \mathbb{E}_{\pi(x_0, x_1)} [\text{KL}(Q_{\pi|x_0, x_1} \| Q_{\pi|x_0, x_1}^{\text{ind}})].$$

Recap that Q_π and Q_π^{ind} are both mixtures of Brownian Bridges. Therefore, $Q_{\pi|x_0, x_1} = Q_{\pi|x_0, x_1}^{\text{ind}} = W_{|x_0, x_1}^\varepsilon$ and $\text{KL}(Q_{\pi|x_0, x_1} \| Q_{\pi|x_0, x_1}^{\text{ind}}) = 0$. Then the following holds:

$$\text{KL}(Q_\pi \| Q_\pi^{\text{ind}}) = \text{KL}(\pi(x_0, x_1) \| \pi(x_0)\pi(x_1)) = \mathbb{E}_{\pi(x_0)} [\text{KL}(Q_{\pi|x_0} \| Q_{\pi|x_0}^{\text{ind}})]. \quad (16)$$

Moreover, processes $Q_{\pi|x_0}$ and $Q_{\pi|x_0}^{\text{ind}}$ are diffusion processes (§2). Then we can apply the Girsanov Theorem from (Léonard, 2012):

$$\text{KL}(Q_{\pi|x_0} \| Q_{\pi|x_0}^{\text{ind}}) = \frac{1}{2\varepsilon} \mathbb{E}_{Q_{\pi|x_0}^{\text{ind}}} \int_0^{1-\delta} \|v_{\text{joint}}^{x_0}(t, X_t) - v_{\text{ind}}^{x_0}(t, X_t)\|^2 dt \quad (17)$$

Now let $\delta \downarrow 0$. The integrand is nonnegative, so the integrals increase with $\delta \downarrow 0$, and by monotone convergence we obtain the same identity with \int_0^1 and combine it with (16):

$$\begin{aligned} \text{KL}(\pi(x_0, x_1) \| \pi(x_0)\pi(x_1)) &= \mathbb{E}_{\pi(x_0)} [\text{KL}(Q_{\pi|x_0} \| Q_{\pi|x_0}^{\text{ind}})] = \\ &= \frac{1}{2\varepsilon} \int_0^1 \mathbb{E}_{q_\pi(x_t, x_0)} [\|v_{\text{joint}}(x_t, t, x_0) - v_{\text{ind}}(x_t, t, x_0)\|^2] dt = I(X_0; X_1), \end{aligned} \quad (18)$$

where drifts v_{joint} and v_{ind} are defined as in (14) and (15) respectively. □

B EXTENSIONS OF OUR METHODOLOGY

In this appendix section we present:

- Appendix B.1. General KL divergence estimation method with proof and discussion.
- Appendix B.2. Differential entropy estimation result with two possible algorithms and discussion.
- Appendix B.3. Experimental illustrations to the entropy estimation algorithm.
- Appendix B.4. Interaction information estimation method.

B.1 KL DIVERGENCE ESTIMATOR

In this section, we present a general result for the unbiased estimation of KL divergence between any two distributions $\pi_1(x), \pi_2(x) \in \mathcal{P}(\mathbb{R}^d)$ through the difference of drifts in the SDE formulation (4) of reciprocal processes induced by these distributions, i.e.:

$$Q_{\pi_1} \stackrel{\text{def}}{=} \int W_{|x_0, x_1}^\epsilon d\pi_1(x_1) dp(x_0), \quad (19)$$

$$Q_{\pi_2} \stackrel{\text{def}}{=} \int W_{|x_0, x_1}^\epsilon d\pi_2(x_1) dp(x_0). \quad (20)$$

Theorem B.1 (KL divergence decomposition). *Consider distributions $\pi_1(x_1), \pi_2(x_1), p(x_0) \in \mathcal{P}(\mathbb{R}^d)$, that satisfy some regularity assumptions (Shi et al., 2023, Appendix C), and reciprocal processes Q_{π_1}, Q_{π_2} induced by distributions $\pi_1(x_1), \pi_2(x_1)$ (19), (20). Then the KL divergence between distributions $\pi_1(x_1)$ and $\pi_2(x_1)$ can be represented in the following way:*

$$\text{KL}(\pi_1(x_1) \| \pi_2(x_1)) = \frac{1}{2\epsilon} \int_0^1 \mathbb{E}_{q_{\pi_1}(x_t, x_0)} [\|v^{\pi_1}(x_t, t, x_0) - v^{\pi_2}(x_t, t, x_0)\|^2] dt, \quad (21)$$

where

$$v^{\pi_1}(x_t, t, x_0) = \mathbb{E}_{q_{\pi_1}(x_1 | x_t, x_0)} \left[\frac{x_1 - x_t}{1 - t} \right], \quad (22)$$

$$v^{\pi_2}(x_t, t, x_0) = \mathbb{E}_{q_{\pi_2}(x_1 | x_t, x_0)} \left[\frac{x_1 - x_t}{1 - t} \right] \quad (23)$$

are the drifts of reciprocal processes Q_{π_1} and Q_{π_2} respectively. Holds for any distribution $p(x_0)$.

Our theorem allows us to estimate $\text{KL}(\pi_1(x) \| \pi_2(x))$ knowing only the drifts $v^{\pi_1}(x_t, t, x_0)$ and $v^{\pi_2}(x_t, t, x_0)$, which can be recovered using conditional bridge matching (§2). Note that the expression (21) is very similar to the expression (13) in (§4.1). Distribution $p(x_0)$, can be considered as part of the design space and optimised for each particular problem.

The KL divergence is a fundamental quantity, and its estimator can have many applications, such as mutual information estimation or entropy estimation using results described in B.2.

Proof. Consider

$$\begin{aligned} \text{KL}(\pi_1(x_1)p(x_0) \| \pi_2(x_1)p(x_0)) &= \underbrace{\text{KL}(p(x_0) \| p(x_0))}_{=0} + \mathbb{E}_{p(x_0)} [\text{KL}(\pi_1(x_1|x_0) \| \pi_2(x_1|x_0))] = \\ &= \mathbb{E}_{p(x_0)} [\text{KL}(\pi_1(x_1) \| \pi_2(x_1))] = \text{KL}(\pi_1(x_1) \| \pi_2(x_1)), \end{aligned}$$

Next to get

$$\text{KL}(\pi_1(x_1)p(x_0) \| \pi_2(x_1)p(x_0)) = \frac{1}{2\epsilon} \int_0^1 \mathbb{E}_{q_{\pi_1}(x_t, x_0)} [\|v^{\pi_1}(x_t, t, x_0) - v^{\pi_2}(x_t, t, x_0)\|^2] dt,$$

one can repeat all the steps that were taken to show:

$$\text{KL}(\pi(x_0, x_1) \|\pi(x_0)\pi(x_1)) = \frac{1}{2\epsilon} \int_0^1 \mathbb{E}_{q_{\pi}(x_t, x_0)} [\|v_{\text{joint}}(x_t, t, x_0) - v_{\text{ind}}(x_t, t, x_0)\|^2] dt,$$

in the proof of Theorem 4.1. □

B.2 DIFFERENTIAL ENTROPY ESTIMATOR

A general result on the information projections and maximum-entropy distributions suggests a way of calculating differential entropy through the KL divergence estimation.

Theorem B.2 (Theorem 6.7 in (Kappen, 2024)). *Let $\phi: \mathbb{R}^n \rightarrow \mathbb{R}^k$ be any measurable function, an absolutely continuous probability distribution $p(x) \in \mathcal{P}(\mathbb{R}^d)$ and define $\alpha \stackrel{\text{def}}{=} \mathbb{E}_p \phi(x)$. Now, for any $\theta \in \mathbb{R}^k$ consider an absolutely continuous probability distribution $q_{\theta} \in \mathcal{P}(\mathbb{R}^d)$ with density:*

$$q_{\theta}(x) = \exp(\langle \theta, \phi(x) \rangle - A(\theta)), \quad A(\theta) = \log \mathbb{E}_{q_{\theta}(x)} e^{\langle \theta, \phi(x) \rangle}.$$

If there exists θ^ such that p is absolutely continuous w.r.t. q_{θ^*} and $\mathbb{E}_{q_{\theta^*}(x)} \phi(x) = \alpha$, then*

$$H(p) = H(q_{\theta^*}) - \text{KL}(p \| q_{\theta^*}),$$

Corollary B.3. *Let X be a d -dimensional absolutely continuous random vector with probability density function p , mean m and covariance matrix Σ . Then*

$$H(p) = H(\mathcal{N}(m, \Sigma)) - \text{KL}(p \| \mathcal{N}(m, \Sigma)), \quad H(\mathcal{N}(m, \Sigma)) = \frac{1}{2} \log((2\pi e)^d \det \Sigma),$$

where $\mathcal{N}(m, \Sigma)$ is a Gaussian distribution of mean m and covariance matrix Σ .

Corollary B.4. *Let X be an absolutely continuous random vector with probability density function p and $\text{supp } X = S$, where S has finite and non-zero Lebesgue measure $\mu(S)$. Then*

$$H(p) = H(U(S)) - \text{KL}(p \| U(S)), \quad H(U(S)) = \log \mu(S),$$

where $U(S)$ is a uniform distribution on S .

Similar results can also be obtained for other members of the exponential family. The first result (B.3) can be considered as a general recipe, while the second one (B.4) can be useful when we have prior knowledge about the support of X being restricted. Approach described in B.2 is very flexible and can be considered as a generalization of the method used in (Franzese et al., 2024).

In practice, to estimate the entropy of some probability distribution, it is sufficient to follow one of the described in B.4 or B.3. For example, if one uses Corollary B.3: 1) estimate mean m and covariance matrix Σ using a set of data samples, 2) calculate entropy $H(\mathcal{N}(m, \Sigma))$ via the closed form expression, 3) calculate the KL divergence $\text{KL}(p \| \mathcal{N}(m, \Sigma))$ via learning two conditional diffusion bridges models and utilizing our estimator (21) from B.1.

B.3 ENTROPY ESTIMATION EXPERIMENTS

We conduct entropy estimation experiments using our method proposed in Section B.2. We estimate the entropy of high-dimensional ($D = 10$) exponential and uniform distributions π with varying distribution parameters. Theorem B.3 (Gaussian) method is used for the both distributions and Theorem B.4 (Uniform) method for the uniform distribution, since it has finite support. For each of the setups we prepare the dataset of 8000 training and 2000 test samples. Additionally we explore different reference distributions $p(x_0)$, see Theorem B.1, for the $\text{KL}(\cdot \| \mathcal{N}(m, \Sigma))$ or $\text{KL}(\cdot \| U(S))$ estimation. We explored four reference distributions $p(x_0)$: low ($\epsilon = 0.1$), medium ($\epsilon = 1$), and high ($\epsilon = 10$) variance Gaussians (all with zero mean), and a "data Gaussian" with mean and standard deviation derived from the training data.

One can observe that *InfoBridge* is capable of entropy estimation on practice. Versions with low/medium variance gaussians generally show superior performance to high variance gaussian and data gaussian. In the case of uniform distribution (Theorem B.4) method performs a lot better, suggesting that it is preferable in the cases when it can be applied (restricted support distributions).

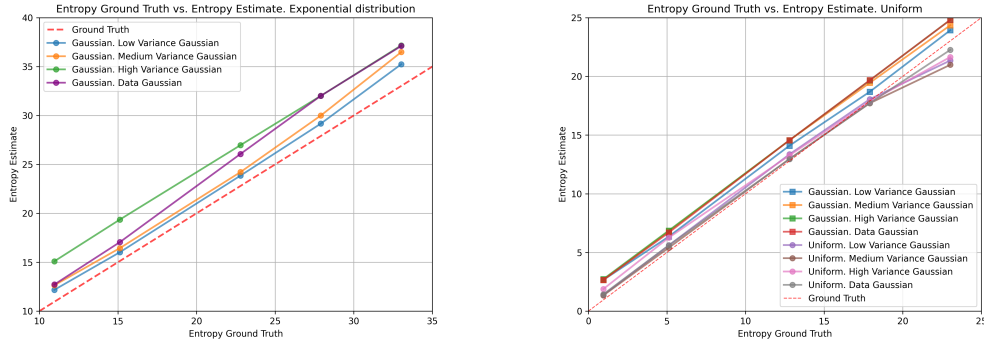


Figure 4: Comparison of our *InfoBridge* combined with different methods Theorem B.3 (Gaussian) and Theorem B.4 (Uniform) and with different reference distributions $p(x_0)$ on the entropy estimation task. Along x axes is the ground truth entropy $H(X)$, along y axes is the entropy estimate $\hat{H}(X)$. Each configuration is ran once.

B.4 INTERACTION INFORMATION

Here we propose the generalization of *InfoBridge* for the *interaction information* estimation, which is the generalization of mutual information for more than two random variables (Rosas et al., 2019). Interaction information for random variables X_0, X_1, X_2 is defined by:

$$\begin{aligned} I(X_0; X_1; X_2) &\stackrel{\text{def}}{=} I(X_0; X_1) - I(X_0; X_1|X_2) = \\ &= \text{KL}(\Pi_{X_0, X_1} \| \Pi_{X_0} \otimes \Pi_{X_1}) - \text{KL}(\Pi_{X_0, X_1|X_2} \| \Pi_{X_0|X_2} \otimes \Pi_{X_1|X_2}). \end{aligned} \quad (24)$$

This definition can be generalized for more random variables in a similar way. Both MI information terms can be estimated using Theorem 4.1 and our practical algorithm *InfoBridge*. Applications of interaction information include neuroscience (Bounoua et al., 2024b), climate models (Runge et al., 2019), econometrics (Dosi & Roventini, 2019).

B.5 MUTUAL INFORMATION BETWEEN RANDOM VARIABLES OF DIFFERENT DIMENSIONALITY

Here we outline the ways to estimate the mutual information between variables of different dimension. In turn this allows to calculate the mutual information between random variables from different modalities, e.g., text and images.

- **Zero or noise padding.** One can embed the lower dimensional variable into the higher dimensional space by padding the spare dimensions with zeros or noise. Such padding does not affect the mutual information, as (1) the padding can be decoupled from the original random variable, and (2) it remains uncorrelated with the other random variables.
- **Employ the general KL estimation result.** One can employ our general KL estimation result, i.e., Theorem B.1. There, we propose to add a third distribution, e.g., a point, normal distribution, or distribution of images, to start our two diffusion bridge matching models from. One can set $\pi_1(x) = q(x_1, x_2)$ and $\pi_2(x) = q_1(x_1)q_2(x_2)$, where x_1 and x_2 random variables of different dimension, i.e., $x_1 \in \mathbb{R}^{d_1}$ and $x_2 \in \mathbb{R}^{d_2}$.
- **Autoencoder-based latent alignment.** Another approach is to embed both random variables into a common latent space via autoencoders. Since a properly trained autoencoder preserves mutual information (Butakov et al., 2024b), MI estimation can then be carried out in this shared latent space.

C ADDITIONAL DISCUSSION ON METHOD

C.1 CONCEPTUAL COMPARISON WITH MINDE

While MINDE also utilizes diffusion models for the MI estimation task, our method is built with totally different diffusion processes in mind. Utilization of regular diffusion generative modeling processes in MINDE has several disadvantages that our method particularly addresses.

First, by leveraging finite-time bridge processes instead of infinite-time diffusion (which in practice is approximated with a finite-time horizon), we provide an **unbiased** estimator. In particular, one can see that the MINDE MI estimator (9) has an intractable bias term in it, i.e., $\text{KL}(q_T^A \| q_T^B)$, while our MI estimator (13) is exact.

Second, MINDE treats MI estimation as a **generative modeling task**, learning drifts to transform $\mathcal{N}(0, I)$ into Π_{X_1} or $\Pi_{X_1|X_0}$. In contrast, our method frames it as a **domain transfer task**, directly transforming input marginal Π_{X_0} to distributions $\Pi_{X_1|X_0}$ or Π_{X_1} . This lead to two consequences:

- In domain transfer the diffusion bridge process is *easier to learn*, since it both starts and ends at data. This is a contrast to complex generation diffusion process that starts at noise and ends at data. The diffusion bridge approaches for domain transfer with diffusion process starting at data are known to be superior to conditional diffusion models (Liu et al., 2023; Zhou et al., 2024).
- In our method each of the diffusion process starting at some particular point x_0 is a Schrödinger Föllmer process (Vargas et al., 2023), which is a special instance of Schrodinger Bridge (Bortoli et al., 2024; Vargas et al., 2021). Trajectories of Schrodinger Bridge processes with small volatility coefficient ϵ require less energy for translation and are relatively "straight". As a result, these trajectories are easy to follow, are expected to deliver *less numerical error* when dealt with and are easier to learn.

To *empirically support the mentioned superiorities* of our domain translation trajectories over MINDE’s data generation trajectories, we compute the variance of MI estimation, which is based on trajectory Monte Carlo integration (Eq (13) for our method, Eq 19 (Franzese et al., 2024) for MINDE). Specifically, we evaluate MINDE-C and our method on the image-based benchmark (§ 5.2) using 16×16 rectangular images. We vary the number of sample tuples $\{x_0^i, x_t^i, x_T^i\}_{i=1}^N$ for MINDE-C and $\{x_0^i, x_t^i, x_1^i\}_{i=1}^N$ for our method and run 10 MI estimates per setting, and report the mean \pm standard deviation in Table 3.

Method \ N samples	128	1024	4096	16384	65536	131072
InfoBridge (ours)	9.79 \pm 0.72	9.84 \pm 0.34	9.9 \pm 0.1	9.84 \pm 0.06	9.86 \pm 0.028	9.84 \pm 0.028
MINDE	12.20 \pm 6.65	11.46 \pm 3.32	10.62 \pm 3.94	12.59 \pm 2.53	11.17 \pm 1.38	10.67 \pm 0.75

Table 3: Comparison of MI estimation accuracy across different sample sizes.

Our method achieves *1–2 orders of magnitude lower standard deviation* in MI estimates compared to MINDE. Even with 1000× more samples, MINDE only approaches our accuracy. This is due to its reliance on complex noise-to-data trajectories, which make its estimates highly volatile and unreliable, unlike our more stable data-to-data paths. As shown in Figure 1, MINDE consistently exhibits the largest and most unstable confidence intervals, undermining the reliability and precision of its MI estimates. Furthermore, every sample requires inference of a neural network and hence the reliable estimation of MI by MINDE requires several orders of magnitude more computational resources.

C.2 ABLATION STUDY

Here we vary different important hyperparameters of our *InfoBridge* method.

Volatility coefficient ϵ . We evaluate different volatility coefficients on the image benchmark (§5.2) and protein embeddings data (§5.3). We run the image benchmark experiment on Gaussian 16x16 setting with ground truth MI=10 and the full protein embeddings data experiment with one random seed and report mean MAE (Mean Absolute Error) error for the last 5 measurements during training,

in both of setups. Results are presented in Table 4 and Table 5. One can see that MAE relatively stable for all the setups, while the optimal ϵ values is different for the both experiments.

One can notice that $\epsilon = 1$ works relatively well on both of the setups. Furthermore, $\epsilon = 1$ performs well on all the experiments we have done, we use it for the three out of four experiments in the main part of the paper and show its competitiveness on the high MI experiment in Appendix D.5. In that light we call $\epsilon = 1$ a **robust choice** suitable for all the data.

We consider ϵ hyperparameter as a tool for **bias/variance trade-off**. The bigger ϵ hyperparameter corresponds to the reduction of variance and growth of bias, i.e., the learning procedure is very stable but slow, MI is mostly underestimated, and the method is stable w.r.t. other hyperparameters. While a smaller ϵ hyperparameter corresponds to the growth of variance and reduction in bias, i.e., the learning procedure has more variance but converges faster, and the model is less stable w.r.t. other hyperparameters. The general advice is to take ϵ as low as possible to keep the learning procedure stable. In most cases, $\epsilon = 1$ is enough to get decent results and keep the model stable.

Table 4: Mean Absolute Error (MAE) values on Image data benchmark (Gaussian 16x16) with ground truth MI=10 experiment for the different ϵ values. Each configuration (except for $\epsilon = 1$) is ran one time and 5 last MI measurements during training are averaged to produce the shown result. The best configuration is **bolded** and configuration used in the main part of the paper is underlined.

ϵ	0.001	0.003	0.01	0.03	0.1	0.3	1	3	10
MAE ↓	2.09	1.79	1.53	1.53	1.72	1.79	<u>2.46</u>	2.82	6.45

Table 5: Mean Absolute Error (MAE) values on ProfTran5 experiment, averaged over all the ground truth MI values, for the different ϵ values. Each configuration (except for $\epsilon = 1$) is ran one time and 5 last MI measurements during training are averaged to produce the shown result. The best configuration is **bolded** and configuration used in the main part of the paper is underlined.

ϵ	0.1	0.3	1	3	10
MAE ↓	0.775	0.232	0.04	0.089	0.129

Number of parameters in a neural network. The width of the Unet (Ronneberger et al., 2015) neural network architecture used in *InfoBridge* on Image benchmark experiments is varied to yield different number of parameters of a neural network. Numbers of base filters, 256, 64, 32, 16, 8, yield number of parameters, 27M, 1.7M, 428K, 108k, 28k. Each configuration, except for 256 number of filters and 27M parameters is run once, and the final five mutual information (MI) measurements during training are averaged to obtain the reported results. Outcomes are presented in Table 6. As one can see our *InfoBridge* is robust w.r.t. neural network architecture.

Table 6: Comparison of the *InfoBridge* with different neural network architectures on the Image data benchmark (16×16 Gaussians setup) with ground truth MI=7.5. Each configuration is ran one time and 5 last MI measurements during training are averaged to produce the shown result. The configuration used in the main experimental part is underlined.

N Params	GT MI=7.5 (mean ± std)
28k	7.56 ± 0.3
108k	6.67 ± 0.15
428k	6.67 ± 0.13
1.7M	6.52 ± 0.07
<u>27M</u>	6.59 ± 0.17

Training dynamics. Here we show the training dynamics of our *InfoBridge* on the High MI experiment within the Smoothed Uniform distributions setup from Section 5.4. Originally we train our model for 200 epochs and the Table shows the MI estimation on the different stages of training:

10, 20, 30, 60, 120, 200 epochs. The results are presented in Table 7. One can see that our method is **robust** w.r.t. number of training iterations or number of training epochs used.

N epochs	GT MI	10	20	40	80
10		8.14	16.09	30.87	47.70
20		7.79	15.51	30.26	48.61
30		7.70	15.50	30.47	50.16
60		7.51	15.02	29.67	50.20
120		7.29	14.63	29.55	50.01
200		7.01	14.32	28.89	50.82

Table 7: The MI estimation of ours *InfoBridge* method is shown for different training stages. The experimental setup is High MI test with Smoothed Uniform distributions. The same 10, 20, 40, 80 MI distributions, as in the main text are used.

C.3 TRAIN SAMPLE SIZE STUDY

Here we study the stability of our *InfoBridge* method w.r.t. the size of train dataset. While in main text we study datasets that do consist of 100k train samples in all the cases except for protein data experiment Section 5.3, in this section we test lower train samples sizes of 5k and 10k.

In particular, we take the Rectangle 16×16 experiments setup from Section 5.2, where we do vary the number of training samples: 100k, 10k and 5k. The number of test samples is the same 10k. The results from 100k are taken directly from the original experiment in Section 5.2. For MINDE and our *InfoBridge* methods we do make neural networks smaller to prevent overfitting.

Method	N train samples	N params	MAE	0.1	1	2.5	5	7.5	10
InfoBridge (ours)	5k	106k	0.199	0.008	0.79	2.33	4.83	7.20	9.75
MINDE	5k	106k	2.397	0.47	0.36	0.44	0.38	4.90	5.91
MINE	5k	50k	1.618	0.00	0.60	2.00	3.74	4.77	5.28
InfoBridge (ours)	10k	428k	0.142	0.006	1.02	2.65	5.24	7.65	9.80
MINDE	10k	428k	1.663	0.46	0.44	0.48	5.93	6.93	4.46
MINE	10k	50k	1.513	0.00	0.78	2.10	3.90	4.85	5.39
InfoBridge (ours)	100k	27M	0.228	0.00	1.16	2.79	5.47	7.67	9.82
MINDE	100k	27M	0.815	0.41	0.91	2.45	4.22	5.63	8.21
MINE	100k	50k	0.978	0.47	1.15	2.43	4.41	5.86	6.95

Table 8: Image benchmark experiment with Rectangle 16×16 setup with variable train samples size. MAE stands for Mean Absolute Error. The best method along each N train samples setup is **bolded**.

The results are presented in Table 8. One can see that our method’s performance stays almost the same, while MINDE and MINE performance degrade. This shows the robustness of our method w.r.t. the size of train dataset.

C.4 STRATEGIES FOR DRAWING TRAIN SAMPLES

Here we explore several design choices for sampling the data utilized for computation of the independent drift function loss \mathcal{L}_θ^2 in the Algorithm 1. In (Letizia et al., 2024) authors argue that **independent permutation** used in the Algorithm 1 introduces additional correlation. In practice, even the simplest one as regular permutation works well, but it can be replaced by either **”derangement”** permutation (Letizia et al., 2024) or **new marginal draws**.

We test these strategies on the High MI experiment with the Smoothed Uniform distribution. All the ours *InfoBridge* method hyperparameters (except for the training data sampling method) match the ones used in the main text. The results are presented in Table 9 and show a **slight performance improvement** for both derangement and fresh marginal draws strategies across all the setups.

Samples draw strategy	MAE	MI=10	MI=20	MI=40	MI=80
Independent Permutation*	12.24	7.01	14.32	28.89	50.82
Derangement	10.51	7.24	14.74	31.21	54.78
Fresh sample draw	10.62	7.31	14.76	30.06	55.38

Table 9: Study on methods for drawing independent samples for the computation of \mathcal{L}_θ^2 in Algorithm 1. The experiment setup is High MI (see Section 5.4) with Smoothed Uniform distributions. * - states for method used in the main paper experiments. In the top MI states for ground truth MI and the closer results to the ground truth the better. The best MI estimation is **bolded** for each MI setup.

C.5 ONE NEURAL NETWORK APPROACH VERSUS TWO NEURAL NETWORKS APPROACH

In this section, we empirically justify the one neural network choice described in Section 4.2. In particular, we take Image Data experiment Rectangle 16×16 setup from Section 5.2 and try two drift functions parameterizations: 1) **one neural network approach** described in Section 4.2 and 2) **two neural networks approach** where each v_{joint} and v_{ind} parametrized by different neural networks. Both approaches have hyperparameters that do match ones used for the experiment in the Section 5.2 fully. The results are presented in Table 10. One can see that the two neural networks approach consistently overestimates the MI and generally provides more error. That is why we stick to the one neural network approach.

Model	GT MI=0.1	GT MI=1	GT MI=2.5	GT MI=5	GT MI=7.5	GT MI=10
One Neural Network	0.00	1.16	2.79	5.47	7.67	9.82
Two Neural Networks	0.83	1.86	3.49	5.93	8.12	10.23

Table 10: The comparison between the parametrizations for drift functions v_{joint} and v_{ind} , i.e., one neural network approach and two neural networks approach. The comparison is done on Image Data benchmark Rectangle 16×16 setup. The table shows MI estimation and GT MI in the top row stands for ground truth MI. The best result along each setup is **bolded**.

D EXPERIMENTAL SUPPLEMENTARY

In this section, additional experimental results and experimental details are described.

D.1 METRICS

MAE. Mean Absolute Error (MAE) is computed as follows:

$$\text{MAE}(x, y) = |x - y|.$$

We measure the MAE between MI estimates and ground truth MI values. In Image Data benchmark analysis Table 2 the MAE is shown averaged over all of the experiments including the different seed runs. In Appendix C.2 Ablation study Table 4 the MAE is averaged over last 5 MI estimations during training and in Table 5 the MAE averaged over all the experimental setups and 5 last MI estimations during training.

Std. Standard deviation (std) is computed over samples as follows:

$$\text{std}(\{x_i\}_{i=0}^N) = \sqrt{\frac{1}{N-1} \sum_{i=0}^N (x_i - \bar{x})^2},$$

where $\bar{x} = \frac{1}{N} \sum_{i=0}^N x_i$.

Table 11: Neural networks hyperparameters for low-dimensional (Czyż et al., 2023) benchmark. “Dim” - dimensionality of a MI estimation problem, “Filters” – number of filters in MLP, “Time Embed” – number filters in time embedding, “Parameters” – number of overall neural network parameters.

Dim	Filters	Time Embed	Parameters
≤ 5	64	64	43K
25	128	128	176K
50	256	256	699K

D.2 LOW-DIMENSIONAL BENCHMARK

Additional results. In Table 21 we present the results of low-dimensional benchmark (Czyż et al., 2023) with precision of 0.01 nats.

Experimental details. The benchmark implementation is taken from the official repository:

<https://github.com/cbg-ethz/bmi>

InfoBridge. Neural networks are taken of almost the same architecture as in (Franzese et al., 2024), which is MLP with residual connections and time embedding. Additional input s described in (§ 4.2) and is processed the same way as time input. Number of parameters is taken depending on a dimensionality of the problem, see Table 11. Exponential Moving Average as a widely recognized training stabilization method was used with decay parameter of 0.999. For all the problems neural networks are trained during 100k iterations with $\epsilon = 1$, batch size 512, lr 0.0003. Mutual Information is estimated by Algorithm 2 with N pairs of samples $\{x_t^i, x_0^i, t^i\}_{i=1}^N$, where N is equal to the number of test samples times 10, i.e., 100k. The time t is sampled uniformly in $t \in [0, 1 - 10^{-3})$ segment. The approximate runtime was under the 20 minutes for each of the experimental setup on NVIDIA A100 GPU.

NVF and JVF. The implementation of NVF and JVF is taken from the official repository:

<https://github.com/calebdahlke/FlowMI>

and used with all the provided by authors default hyperparameters for the benchmark. The methods are ran on CPU and execution takes less then two hours for each benchmark problem run. The size of a neural network is from 10k to 400k parameters depending of the task dimensionality and the submethod. The approximate runtime was under the 30 minutes under the 30 minutes for NVF and under the 1 hours for JVF for each of the experimental setup on NVIDIA A100 GPU.

D.3 IMAGE DATA BENCHMARK

Random seeds. We run *InfoBridge*, MIENF, and MINDE with 3 random seeds, and all other methods with 5 seeds per experimental setup. In Figure 1 and Table 2, we report the mean performance across seeds, along with standard deviations and confidence intervals computed from the seed-wise variability.

Experimental details for *InfoBridge*. The implementation of image data benchmark (Butakov et al., 2024a) was taken from the official repository:

<https://github.com/VanessB/mutinfo>

Following authors of the benchmark, *Gaussian* images were generated with all the default settings, *Rectangle* images were also generated with all the default settings, but minimum size of rectangle is 0.2 to avoid singularities. All the covariance matrices for the distributions defining the mutual information in the benchmark were generated without randomization of component-wise mutual information, but with randomization of the off-diagonal blocks of the covariance matrix.

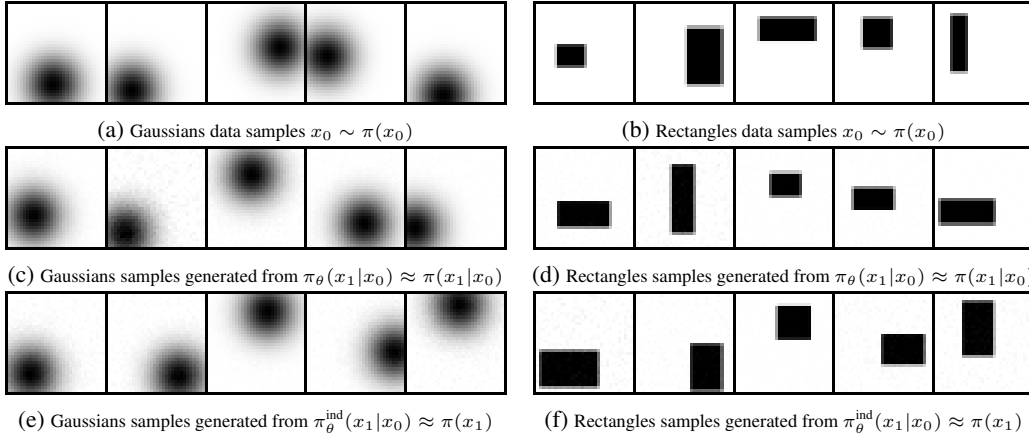


Figure 5: Examples of synthetic images from the (Butakov et al., 2024a) benchmark can be seen in Figures 5a and 5b. Note that images are high-dimensional, but admit latent structure, which is similar to real datasets. Samples generated by our *InfoBridge* from the learned distributions $\pi_\theta(x_1|x_0) \approx \pi(x_1|x_0)$ and $\pi_\theta^{\text{ind}}(x_1|x_0) \approx \pi(x_1)$ defined as solutions to SDEs (4) with approximated drifts $v_\theta(\cdot, 0)$ and $v_\theta(\cdot, 1)$, respectively, can be seen in Figures 5c to 5f. All the images have 32×32 resolution.

To approximate the drift coefficient of diffusion U-Net (Ronneberger et al., 2015) with time, conditional neural networks were used, special input s was processed as time input. For all the tests, neural networks were the same and had 2 residual layers per U-net block with 256 base channels, positional timestep encoding, upscale and downscale blocks consisting of two resnet blocks, one with attention and one without attention. The number of parameters is $\sim 27\text{M}$. During the training, 100k gradient steps were made with batch size of 64 and learning rate 0.0001. Exponential moving average was used with decay rate 0.999. Mutual Information was estimated by Algorithm 2 with N pairs of samples $\{x_t^n, x_0^n, t^n\}_{i=n}^N$, where N is equal to the number of test samples, i.e., 10k. Nvidia A100 was used for the *InfoBridge* training. Each run (one seed) took around 6 and 18 GPU-hours for the 16×16 and 32×32 image resolution setups, respectively. The time t is sampled uniformly in $t \in [0, 1 - 10^{-3}]$ segment.

Visualization of learned distribution. Figure 5 presents samples generated from the learned distributions alongside ground truth samples from the dataset. It is evident that the samples from both $\pi_\theta(x_1|x_0)$ and $\pi_\theta^{\text{ind}}(x_1|x_0)$ closely resemble those drawn from $\pi(x_0)$, indicating that the marginal distribution of x_0 is well approximated by the learned models.

Experimental details for other methods. In this part, we provide additional experimental details regarding other methods featured in Figure 1. We report the NN architectures used for neural estimators in Table 12.

Table 12: The NN architectures used to conduct the tests with images in 5.

NN	Architecture
GLOW, 16×16 (32×32) images	$\times 1$: 4 (5) splits, 2 GLOW blocks between splits, $\times 2$ in parallel 16 hidden channels in each block, leaky constant = 0.01
	$\times 1$: Orthogonal projection linear layer $\times 2$ in parallel
Critic NN, 16×16 (32×32) images	$\times 1$: [Conv2d(1, 16, ks=3), MaxPool2d(2), LeakyReLU(0.01)] $\times 2$ in parallel
	$\times 1(2)$: [Conv2d(16, 16, ks=3), MaxPool2d(2), LeakyReLU(0.01)] $\times 2$ in parallel
	$\times 1$: Dense(256, 128), LeakyReLU(0.01)
	$\times 1$: Dense(128, 128), LeakyReLU(0.01)
	$\times 1$: Dense(128, 1)

MINDE. We use the official implementation of MINDE:

<https://github.com/MustaphaBounoua/minde>

As a neural network, we adapt same U-net architecture as for our *InfoBridge* in image data experiments with approximately the same number of parameters , i.e., 27M. Training procedure hyperparameters do match the *InfoBridge*, i.e., 100k gradient steps with batch size 64 and learning rate 0.0001, exponential moving average with 0.999 decay rate. Mutual Information was estimated using 10 samples of $\{t^i, x_t^i\}$ per each pair $\{x_0^i, x_1^i\}$ in the test dataset. Nvidia A100 was used to train the models. Each run (one seed) took around 2 and 5 GPU-hours for the 16×16 and 32×32 image resolution setups.

MIENF. Under MIENF we consider gaussian-based \mathcal{N} -MIENF. This method is based on bi-gaussianization of the input data via a Cartesian product of learnable diffeomorphisms (Butakov et al., 2024a). Such approach allows for a closed-form expression to be employed to estimate the MI.

With only minor stability-increasing changes introduced, we adopt the Glow (Kingma & Dhariwal, 2018) flow network architecture from (Butakov et al., 2024a), which is also reported in 12 (“GLOW”). We used the `normflows` package (Stimper et al., 2023) to implement the model. Adam (Kingma & Ba, 2017) optimizer was used to train the network on 10^5 images with a batch size 512, and the learning rate decreasing from $5 \cdot 10^{-4}$ to 10^{-5} geometrically. For averaging, we used 3 different seeds. Nvidia A100 was used to train the flow models. Each run (one seed) took no longer than four GPU-hours to be completed. The size of normalizing flow neural network is around 200k parameters.

KSG. Kraskov-Stögbauer-Grassberger (Kraskov et al., 2004) mutual information estimator is a well-known k -NN non-parametric method, which is very similar to unweighted Kozachenko-Leonenko estimator (Kozachenko & Leonenko, 1987). This method employs distances to k -th nearest neighbors to approximate the pointwise mutual information, which is then averaged.

We used $k = 1$ (one nearest neighbour) for all the tests. The number of samples was 10^5 for Gaussian images and 10^4 for images of rectangles (we had to lower the sampling size due to degenerated performance of the metric tree-based k -NN search in this particular setup). A single core of AMD EPYC 7543 CPU was used for nearest neighbors search and MI calculation. Each run (one seed) took no longer than one CPU-hour to be completed.

MINE, NWJ, InfoNCE. These discriminative approaches are fundamentally alike: each method estimates mutual information by maximizing the associated KL-divergence bound:

$$I(X_0; X_1) = \text{KL}(\pi(x_0, x_1) \parallel \pi(x_0)\pi(x_1)) \geq \sup_{T: \mathbb{R}^d \times \mathbb{R}^d \rightarrow \mathbb{R}} \mathbb{F}[T(x_0, x_1)], \quad (25)$$

where T is measurable, and \mathbb{F} is some method-specific functional. In practice, T is approximated via a neural network, with the right-hand-side in (25) being used as the loss function.

Motivated by this similarity, we use a nearly identical experimental framework to assess each approach within this category. To approximate T in experiments with synthetic images, we adopt the critic NN architecture from (Butakov et al., 2024a), which we also report in Table 12 (“Critic NN”).

The networks were trained via Adam optimizer on 10^5 images with a learning rate 10^{-3} , a batch size 512 (with InfoNCE being the only exception, for which we used batch size 256 for training and 512 for evaluation due to memory constraints), and MAE loss for 10^5 steps. For averaging, we used 5 different seeds. Nvidia A100 was used to train the models. In any setup, each run (one seed) took no longer than two GPU-hours to be completed. The size of discriminator neural network is around 50k parameters.

AE-WKL Baseline. Here we include an additional baseline Auto Encoder + Weighted Kozachenko-Leonenko (AE-WKL) for the image based benchmark, which we exclude from the main part of the paper due to instability w.r.t. hyperparameters and huge inductive bias.

The idea of leveraging lossy compression to tackle the curse of dimensionality and provide better MI estimates is well-explored in the literature (Goldfeld & Greenwald, 2021; Goldfeld et al., 2022; Tsur et al., 2023; Fayad & Ibrahim, 2023; Greenwald et al., 2023; Butakov et al., 2024b). In our work, we adopt the non-linear compression setup from (Butakov et al., 2024b), which employs autoencoders for data compression and weighted Kozachenko-Leonenko method (Berrett et al., 2019) for MI estimation in the latent space.

However in this approach non-parametric MI estimator (WKL) approach **heavily relies on the autoencoder latent space**.

First, prior works suggest that non-parametric MI estimators are highly prone to the curse of dimensionality compared to NN-based approaches (Goldfeld et al., 2020; Czyż et al., 2023; Butakov et al., 2024a) and hence WKL performance seriously deteriorates with growth of latent space dimensionality. In particular, Figures 2 and 3 in (Goldfeld et al., 2020) and Table 1 in (Butakov et al., 2024a) indicate that weighted Kozachenko-Leonenko estimator fails to yield reasonable estimates at all if the dimensionality reaches certain threshold.

Second, the performance of estimator depends on the amount of information preserved in the latent space by the autoencoder. If the dimension of latent space is less than dimension of the data manifold, the performance of the method should deteriorate as well.

We validate the AE-WKL approach with different dimensionality of autoencoder latent space in the Gaussian images setup. We increase the latent space dimensionality from $d = 2$ (which is the intrinsic dimensionality of the dataset in question) to $d \in \{4, 5, 8\}$. We report our results in Figure 6. One can see while with $d = 2$ latent space (which is the true latent dimensionality of gaussian images) AE-WKL approach achieves remarkable results, but with growth of dimension to $d \in \{4, 5, 8\}$ the performance starts to deteriorate with $d = 8$ even leading to exploded estimates.

That leaves autoencoder approaches combined with non parametric MI estimators highly dependent on the successful latent space choice. This choice is trivial on the image based benchmark, where the dimensionality of data manifold is known by construction, however such information is usually unknown in real world scenario, which makes approaches like AE-WKL highly unreliable.

The autoencoders were trained using Adam optimizer on 10^5 images with a batch size 512, a learning rate 10^{-3} and MAE loss for 10^4 steps. For averaging, we used 5 different seeds. Nvidia A100 was used to train the autoencoder model. Each run (one seed) took no longer than one GPU-hour to be completed.

Runtime comparisons One can see the approximate runtime comparisons between the featured methods in Table 13.

Method	Runtime	Hardware
InfoBridge	6 hours	GPU
MINDE	2 hours	GPU
MIENF	4 hours	GPU
InfoNCE	1 hour	GPU
MINE	1 hour	GPU
NWJ	1 hour	GPU
KSG	1 hour	CPU

Table 13: Comparison of methods approximate runtime on the Image benchmark 16×16 . GPU states for NVIDIA A100.

D.4 PROTEIN EMBEDDINGS DATA

Table 14: The best result is **bolded and underlined** and second best result is **bolded**.

Method	InfoBridge	MINE	InfoNCE	KSG	MINDE-C	MINDE-J
MAE ↓	<u>0.04</u>	0.223	0.237	0.116	9.29	1342
MAE Std	0.01	0.017	0.007	-	1.1	57

Data. We use the UniProt database proteins, their embeddings from prottrans_t5_xl_u50 (Elnaggar et al., 2021) model and download them from <https://github.com/ggdna/latent-mutual-information>. All proteins longer than $12 \cdot 10^3$ residues are excluded. These embeddings are then unit variance normalized. The final number of each protein embeddings (samples) used for training is 20641 and the dimensionality is 1024.

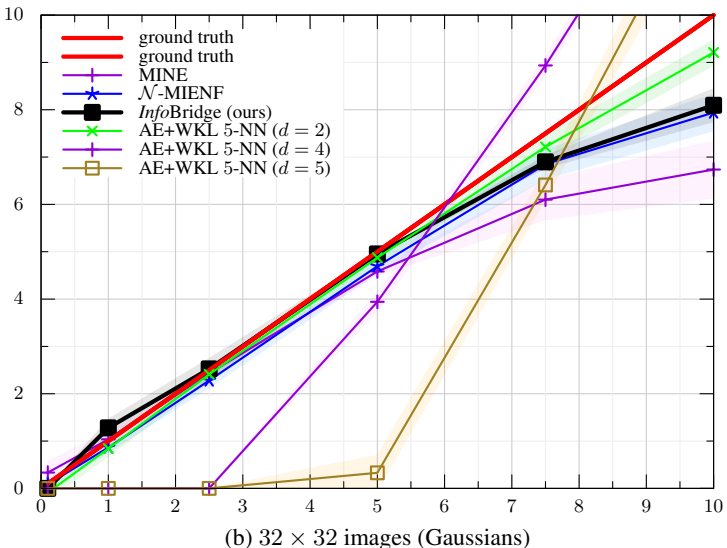
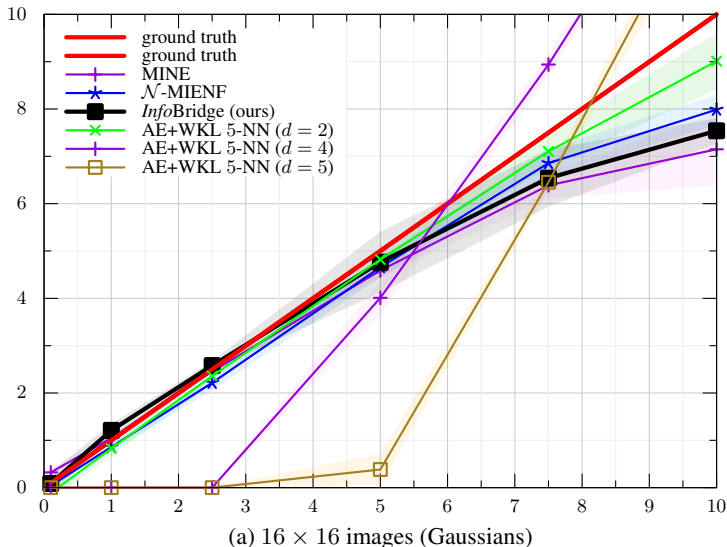


Figure 6: Comparison of the MI estimators. Along x axes is $I(X_0; X_1)$, along y axes is MI estimate $\hat{I}(X_0; X_1)$. We plot 99% confidence intervals acquired from different seed runs.

Methods implementation.

InfoBridge. Hyperparameters are the same as for low-dimensional benchmark Appendix D.2, MLP has $\sim 900k$ parameters, weight decay is 0.001, dropout is 0.2 and the model is trained for 100 epochs. Results for InfoBridge averaged over last 5 MI estimations during training. The size of neural network is around 900k parameters. The time t is sampled uniformly in $t \in [0, 1 - 10^{-3}]$ segment.

MINDE. We leverage the official implementation of MINDE <https://github.com/MustaphaBounoua/minde> in the configuration used for the low-dimensional benchmark, with $\sim 900k$ parameters MLP, lr $1e - 4$, batch size of 256, ema decay of 0.999 and train model for 100 epochs.

MINE, InfoNCE. These estimators are taken from the *bmi* library <https://github.com/cbg-ethz/bmi> with all the default parameters. The size of discriminator neural network is around 1k parameters.

KSG. Implementation is taken from <https://github.com/ggdna/latent-mutual-information> and used with all the default parameters on 20000 training samples.

All the neural methods were trained on Nvidia A100 and took less then one GPU-hour to complete. KSG estimation algorithm took approximately one hour to complete.

Runtime comparisons. One can see the approximate runtime comparisons between the featured methods in Table 15.

Method	Runtime	Hardware
InfoBridge	20 minutes	GPU
MINDE	3 minutes	GPU
MINE	1 minute	CPU
InfoNCE	1 minute	CPU
KSG	20 minutes	CPU

Table 15: Comparison of methods approximate runtime on the Protein Data experiments. GPU states for NVIDIA A100.

D.5 HIGH MUTUAL INFORMATION EXPERIMENTS

Half Cube transform. We adopt the half-cube transform for Gaussian random variables as introduced in (Czyż et al., 2023):

$$f(x) = x\sqrt{|x|}.$$

This transform lengthens the tails of Gaussian random variables, while preserving the MI due to $f(x)$ transform being reversible.

Additional experimental results. In addition to the high MI experiment in the main text (§ 5.4) here we present extended comparisons with other baselines: see Table 16 for Gaussian random variables, Table 17 for Gaussian random variables with half cube transform, Table 18 for Correlated Uniform random variables, Table 19 for Smoothed Uniform random variables. Overall our method still is the most reliable and accurate of the bunch.

As shown, our method performs well with both $\epsilon = 1$ and $\epsilon = 0.01$, with the latter providing slightly better results. For this reason, we adopt $\epsilon = 0.01$ in the main text comparisons.

One can see that MINDE-J offers the closest to the ground truth MI in many setups, but we note that it *drastically overestimates* the MI in the $d=160$, $MI=80$ setup across all the distribution types. Such behaviour is typical for MINDE-J on complex datasets also, see (§ 5.2) and (§ 5.3) that is why we leave it out in the main text comparisons in (§ 5.4).

Method	d=20, MI=10	d=40, MI=20	d=80, MI=40	d=160, MI=80
InfoBridge (ours, $\epsilon = 1$)	9.85	19.99	39.31	<u>78.86</u>
InfoBridge (ours, $\epsilon = 0.01$) [†]	10.35	21.79	<u>41.92</u>	79.76
MINDE-C [†]	9.59	16.96	35.51	56.27
MINDE-J	<u>10.23</u>	<u>20.02</u>	42.11	450
MINE [†]	6.51	8.43	7.76	8.08
InfoNCE [†]	5.14	5.40	4.76	3.80
fDIME (KL, J)	5.51		2.49	0.0
fDIME (HD, J)	5.24	3.66	1.14	0.0
fDIME (GAN, J) [†]	6.88	6.71	3.54	0.0
fDIME (KL, D)	3.71	4.06	0.22	0.0
fDIME (HD, D)	4.01	4.24	0.23	0.0
fDIME (GAN, D)	4.5	4.86	0.32	0.0

Table 16: Mutual Information estimates across increasing dimensions and mutual information levels for the Gaussian random variables. Best MI estimation is **bolded** and second best is underlined. [†] stands for method shown in the high MI experiment in the main text. Empty cell stands for method explosion.

Experimental Details. We use 100k train samples dataset and 10k test dataset for all the methods. Datasets are generated using *mutinfo* library github repository:

Method	d=20, MI=10	d=40, MI=20	d=80, MI=40	d=160, MI=80
InfoBridge (ours, $\epsilon = 1$)	9.07	<u>18.23</u>	34.35	<u>61.63</u>
InfoBridge (ours, $\epsilon = 0.01$) [†]	9.92	20.69	39.6	84.24
MINDE-C [†]	8.31	14.69	33.64	40.63
MINDE-J	<u>9.28</u>	16.49	<u>43.3</u>	308
MINE [†]	3.18	3.0	3.28	3.74
InfoNCE [†]	4.11	4.7	3.84	2.74
fDIME (KL, J)	7.52	6.84	11.3	8.18
fDIME (HD, J)	6.56	11.59	10.77	10.73
fDIME (GAN, J) [†]	9.7	14.7	20.84	13.91
fDIME (KL, D)	5.41	6.82	6.67	6.76
fDIME (HD, D)	5.71	7.66	7.99	8.74
fDIME (GAN, D)	7.83	10.4	11.49	10.86

Table 17: Mutual Information estimates across increasing dimensions and mutual information levels for the Half Cube transformed Gaussian random variables. Best MI estimation is **bolded** and second best is underlined. [†] stands for method shown in the high MI experiment in the main text.

Method	d=20, MI=10	d=40, MI=20	d=80, MI=40	d=160, MI=80
InfoBridge (ours, $\epsilon = 1$)	7.95	15.15	28.46	41.9
InfoBridge [†] (ours, $\epsilon = 0.01$)	<u>8.65</u>	<u>16.93</u>	<u>33.69</u>	57.73
MINDE-C [†]	8.03	15.14	30.78	<u>55.91</u>
MINDE-J	8.8	17.56	34.59	539
MINE [†]	6.12	7.9	7.92	7.11
InfoNCE [†]	4.8	4.48	3.71	3.42
fDIME (KL, J)	7.6		6.1	0.99
fDIME (HD, J)	8.28	8.84	4.8	0.19
fDIME (GAN, J) [†]	9.2	10.33	8.75	1.56
fDIME (KL, D)	5.62	5.1	2.71	0.1
fDIME (HD, D)	6.6	7.02	2.14	0.41
fDIME (GAN, D)	6.49	7.88	3.79	0.0

Table 18: Mutual Information estimates across increasing dimensions and mutual information levels for the Correlated Uniform random variables. Best MI estimation is **bolded** and second best is underlined. [†] stands for method shown in the high MI experiment in the main text.

<https://github.com/VanessB/mutinfo>.

InfoBridge. Implementation was taken with exactly the same hyperparameters as for low-dimensional benchmark experiment, see Appendix D.2.

MINDE. We leverage the official implementation of MINDE <https://github.com/MustaphaBounoua/minde> in the configuration used for the low-dimensional benchmark, with $\sim 900k$ parameters MLP, lr $1e-4$, batch size of 256, ema decay of 0.999 and train model for 100 epochs.

MINE, InfoNCE. These estimators are taken from the *bmi* library <https://github.com/cbg-ethz/bmi> with all the default parameters. The size of discriminator neural network is around 1k parameters.

fDIME. implementation was taken from the official github repository:

<https://github.com/tonellolab/fDIME>,

with all the default hyperparameters. *KL*, *HD*, *GAN* stand for different divergences and *J*, *D* stand for Joint and Derranged architectures of fDIME.

Runtime comparisons. One can see the approximate runtime comparisons between the featured methods in Table 20.

Method	d=20, MI=10	d=40, MI=20	d=80, MI=40	d=160, MI=80
InfoBridge (ours, $\epsilon = 1$)	6.4	12.83	24.21	29.83
InfoBridge (ours, $\epsilon = 0.01$) [†]	7.3	14.63	<u>29.25</u>	50.28
MINDE-C [†]	6.53	13.23	24.98	<u>44.2</u>
MINDE-J	<u>7.63</u>	<u>14.39</u>	31.15	511
MINE [†]	5.56	7.45	7.91	7.17
InfoNCE [†]	3.84	3.67	3.34	3.14
fDIME (KL, J)	6.15	-74	3.09	0.0
fDIME (HD, J)	5.9	8.12	3.95	0.0
fDIME (GAN, J) [†]	7.75	8.49	4.75	0.0
fDIME (KL, D)	4.91	4.17	0.32	0.0
fDIME (HD, D)	4.59	4.82	0.37	0.0
fDIME (GAN, D)	5.65	5.65	0.33	0.0

Table 19: Mutual Information estimates across increasing dimensions and mutual information levels for the Smoothed Uniform random variables. Best MI estimation is **bolded** and second best is underlined. [†] stands for method shown in the high MI experiment in the main text.

Method	Runtime	Hardware
InfoBridge	30 minutes	GPU
MINDE	10 minutes	GPU
f-DIME	1 minute	GPU
MINE	1 minute	CPU
InfoNCE	1 minute	CPU

Table 20: Comparison of methods approximate runtime on the High MI experiments in the $D = 160$, MI=80 case. GPU states for NVIDIA A100.

